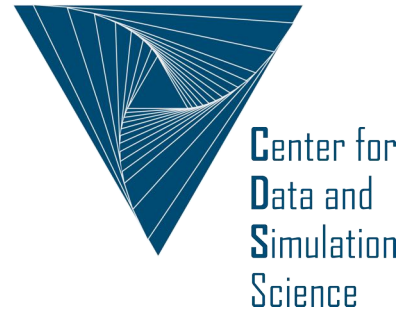


Universität
zu Köln



Technical Report Series Center for Data and Simulation Science

Alexander Heinlein, Axel Klawonn, Jascha Knepper, Oliver Rheinbach, Olof B. Widlund

Adaptive GDSW coarse spaces of reduced dimension for overlapping Schwarz methods

Technical Report ID: CDS-2020-4

Available at <https://kups.ub.uni-koeln.de/id/eprint/12113>

Submitted on September 4, 2020

1 **ADAPTIVE GDSW COARSE SPACES OF REDUCED DIMENSION**
2 **FOR OVERLAPPING SCHWARZ METHODS**

3 ALEXANDER HEINLEIN^{*†}, AXEL KLAWONN^{*†}, JASCHA KNEPPER^{*}, OLIVER
4 RHEINBACH[‡], AND OLOF B. WIDLUND[§]

5 **Abstract.** A new reduced dimension adaptive GDSW (Generalized Dryja-Smith-Widlund)
6 overlapping Schwarz method for linear second-order elliptic problems in three dimensions is in-
7 troduced. It is robust with respect to large contrasts of the coefficients of the partial differential
8 equations. The condition number bound of the new method is shown to be independent of the co-
9 efficient contrast and only dependent on a user-prescribed tolerance. The interface of the nonover-
10 lapping domain decomposition is partitioned into nonoverlapping patches. The new coarse space is
11 obtained by selecting a few eigenvectors of certain local eigenproblems which are defined on these
12 patches. These eigenmodes are energy-minimally extended to the interior of the nonoverlapping
13 subdomains and added to the coarse space. By using a new interface decomposition the reduced
14 dimension adaptive GDSW overlapping Schwarz method usually has a smaller coarse space than
15 existing GDSW and adaptive GDSW domain decomposition methods. A robust condition number
16 estimate is proven for the new reduced dimension adaptive GDSW method which is also valid for
17 existing adaptive GDSW methods. Numerical results for the equations of isotropic linear elasticity
18 in three dimensions confirming the theoretical findings are presented.

19 **Key words.** domain decomposition, multiscale, GDSW, overlapping Schwarz, adaptive coarse
20 spaces, reduced dimension

21 **AMS subject classifications.** 65F08,65F10,65N55,68W10

22 **1. Introduction.** Successful domain decomposition preconditioners for solv-
23 ing elliptic problems all require at least one global, coarse-level component in order
24 to perform satisfactorily if the number of subdomains, into which the given domain
25 has been decomposed, is relatively large. The design and analysis of these coarse
26 components is central in most studies in this field given that they require global
27 communication if the algorithms are implemented on distributed or parallel com-
28 puting systems. In order to avoid creating a bottleneck, it is very important to keep
29 the dimension of the related coarse space small.

30 In recent years, substantial progress has been possible by the development of
31 algorithms which adaptively design the coarse space at a cost of solving local gen-
32 eralized eigenvalue problems. In this paper, we will focus on a particular family
33 of domain decomposition algorithms, the two-level overlapping Schwarz methods,
34 which use one coarse-level component in addition to local components each of which
35 is defined on a subdomain which is part of an overlapping decomposition. We note
36 that the use of adaptively designed coarse spaces has been very successful even with
37 problems with very irregular coefficients; this is clearly demonstrated by examples
38 in [section 14](#) of this paper.

39 The robustness of many coarse spaces for arbitrary coefficient functions is ob-
40 tained by using local generalized eigenvalue problems to adaptively enrich the coarse
41 spaces with suitable basis functions; see, e.g., [[14](#), [10](#), [41](#), [15](#), [20](#), [13](#)]. These ap-
42 proaches differ, e.g., in the sizes of the eigenvalue problems, the coarse space di-
43 mensions, the class of problems considered, and their parallel efficiency. We also

^{*}Department of Mathematics and Computer Science, University of Cologne, Weyertal 86-
90, 50931 Köln, Germany, {[alexander.heinlein](mailto:alexander.heinlein@uni-koeln.de), [axel.klawonn](mailto:axel.klawonn@uni-koeln.de), [jascha.knepper](mailto:jascha.knepper@uni-koeln.de)}@uni-koeln.de, <http://www.numerik.uni-koeln.de>

[†]Center for Data and Simulation Science, University of Cologne, 50931 Köln, Germany, <http://www.cds.uni-koeln.de>

[‡]Institut für Numerische Mathematik und Optimierung, Fakultät für Mathematik und
Informatik, Technische Universität Freiberg, Akademiestr. 6, 09599 Freiberg, oliver.rheinbach@math.tu-freiberg.de, <http://www.mathe.tu-freiberg.de/nmo/mitarbeiter/oliver-rheinbach>

[§]Department of Mathematics, Courant Institute, 251 Mercer Street, New York, NY 10012,
USA, widlund@cims.nyu.edu, <https://cs.nyu.edu/faculty/widlund>

44 mention success with adaptive coarse spaces for nonoverlapping domain decompo-
 45 sition methods; see, e.g., [2, 34, 35, 42, 37, 31, 33, 38, 30, 32, 36].

46 Two-level overlapping Schwarz algorithms were first developed with coarse spa-
 47 ces based on a coarse triangulation of the domain and with subdomains obtained
 48 by adding one or a few layers of fine elements to each coarse mesh element, see [43,
 49 Chapter 3]. On the other hand, the iterative substructuring algorithms, developed
 50 for decompositions of the domain into nonoverlapping subdomains, were immedi-
 51 ately available for quite irregular subdomains such as those that can be obtained by
 52 a mesh partitioner such as METIS [29]; see [43, Chapter 4, 5, and 6]. The iterative
 53 substructuring algorithms have been very successful but they cannot be used unless
 54 submatrices associated with the subdomains are available instead of just a fully
 55 assembled stiffness matrix. This was a main reason why a new family of overlap-
 56 ping Schwarz algorithms was developed, known as the GDSW methods (generalized
 57 Dryja–Smith–Widlund), which borrow their coarse components from [43, Algorithm
 58 5.16]. These ideas were first developed in [5, 6]. The elements of these coarse spaces
 59 are defined by their values on the interface between the subdomains with values
 60 in the interiors defined by energy-minimizing extensions. These algorithms were
 61 further developed for almost incompressible elasticity in two papers [7, 8]; in the
 62 second paper the dimension of the coarse spaces was considerably decreased; see
 63 also [23, 16, 24, 25, 17, 22, 26] for further developments.

64 In this paper, we present an approach of constructing adaptive coarse spaces
 65 for the two-level overlapping Schwarz method [40, 43] based on the adaptive GDSW
 66 (AGDSW) coarse space of [21]. In particular, our focus is on one new coarse space –
 67 the reduced dimension adaptive GDSW (RAGDSW) coarse space – and the reduc-
 68 tion of the coarse space dimension. A proof of a condition number estimate, which
 69 is independent of heterogeneities of the coefficient functions, is given in [sections 10](#)
 70 and [11](#). We note that this proof is based on a more general decomposition of the
 71 interface than the one in [21]; it applies to both, the original AGDSW and the new
 72 RAGDSW coarse space. Supporting numerical results are presented in [section 14](#).

73 In our adaptive algorithms, a user prescribed tolerance directly controls the
 74 condition number of the preconditioned operator and, if this tolerance is chosen as
 75 zero, adaptive GDSW is identical to GDSW and reduced dimension adaptive GDSW
 76 is identical to reduced dimension GDSW, the latter being a variant of GDSW defined
 77 on a specific interface partition of the domain decomposition; cf. [section 8](#).

78 We note that our reduced dimension GDSW coarse space differs from the re-
 79 duced dimension GDSW coarse spaces in [9]. However, they share the same core
 80 idea: GDSW and AGDSW use basis functions associated with coarse nodes, edges,
 81 and faces while the coarse spaces in [9], reduced dimension GDSW, and reduced
 82 dimension adaptive GDSW use basis functions associated only with subdomain
 83 vertices. Generally, this leads to a reduction in the coarse space dimension. See
 84 also [8, 4, 27, 18] for reduced dimension GDSW coarse spaces.

85 We note that many other approaches to constructing coarse spaces exist. Some
 86 borrow the idea from the multiscale finite element method (MsFEM) [28, 12] and
 87 use basis functions of that type in the coarse space; c.f. [1, 3, 15, 20, 13]. However,
 88 the coarse spaces in this paper are not based on MsFEM functions.

89 The outline of the paper is as follows: In [section 2](#), we introduce our model
 90 problem followed by the definition of the two-level additive overlapping Schwarz
 91 methods in [section 3](#). In the following five sections, we introduce four families of
 92 GDSW algorithms. In [section 9](#), we give a quite general description of adaptive
 93 GDSW coarse spaces which covers both adaptive GDSW and reduced dimension
 94 adaptive GDSW; see also [section 12](#) for a variant which is computationally cheaper,
 95 easier to implement and more efficient in a parallel implementation. In [sections 10](#)
 96 and [11](#), we derive a condition number estimate for our new reduced dimension
 97 adaptive GDSW preconditioner. In [section 13](#), we address questions that may arise

TABLE 1

Reference table for some definitions used in this paper (in order of their appearance).

Description of coarse spaces (sections 4–8)		
x^h	finite element node	section 4
\mathcal{P}	nonoverlapping partition of the interface	section 4
$\overline{\Omega}_\xi$	union of the closure of the subdomains adjacent to a $\xi \in \mathcal{P}$	section 5
$\{\xi_i\}_{i=1}^{n_\xi}$	partitioning of a $\xi \in \mathcal{P}$ into nodal equivalence classes	
	structured mesh, structured domain decomposition	eq. (7.1)
	unstructured mesh, unstructured domain decomposition	section 8
$n(x^h)$	index set of subdomains which contain x^h	eq. (8.1)
Theory (sections 9–11)		
n^ξ	index set of subdomains adjacent to a $\xi \in \mathcal{P}$	eq. (9.1)
$z_{\xi \rightarrow G}(\cdot)$	extension by zero from ξ to G	eq. (9.2)
$X^h(\xi)$	$X^h(\xi) := \{v : \xi \rightarrow \mathbb{R}^3\}$	section 9
$\mathcal{H}_{\xi \rightarrow \Omega_\xi}(\cdot)$	energy-minimal extension from ξ to Ω_ξ	eq. (9.3)
$c_\xi(u, v)$	$c_\xi(u, v) := \sum_{i=1}^{n_\xi} c_{\xi_i}(u, v)$	eq. (9.4)
$c_{\xi_i}(u, v)$	$c_{\xi_i}(u, v) := a_{\Omega_{\xi_i}}(z_{\xi_i \rightarrow \Omega_{\xi_i}}(u), z_{\xi_i \rightarrow \Omega_{\xi_i}}(v))$	eq. (9.5)
$\ u\ _{c_\xi}^2$	$\ u\ _{c_\xi}^2 := c_\xi(u, u)$	eq. (9.6)
$\Pi_\xi w$	$\Pi_\xi := \sum_{\lambda_{k,\xi} \leq \text{tol}_\xi} c_\xi(w, v_{k,\xi}) v_{k,\xi}$	eq. (10.1)
$\Pi_{\mathcal{P}} w$	$\Pi_{\mathcal{P}} w := \sum_{\xi \in \mathcal{P}} \Pi_\xi w$	eq. (10.1)
$ u _{d_\xi}$	$ u _{d_\xi} := \sqrt{d_\xi(u, u)}$, $d_\xi(\cdot, \cdot) := a_{\Omega_\xi}(\mathcal{H}_{\xi \rightarrow \Omega_\xi}(\cdot), \mathcal{H}_{\xi \rightarrow \Omega_\xi}(\cdot))$	eq. (10.2)
$ u _{a(B)}$	$ u _{a(B)} := \sqrt{a_B(u, u)}$	eq. (10.3)
C_τ	max. number of vertices of a finite element	Lemma 11.2
$\mathcal{P}(\Omega_i)$	$\xi \in \mathcal{P}$ adjacent to subdomain i	eq. (11.1)
N^ξ	max. number of $\xi \in \mathcal{P}$ adjacent to a subdomain	eq. (11.1)
$\text{tol}_{\mathcal{P}}$	$\text{tol}_{\mathcal{P}} := \min_{\xi \in \mathcal{P}} \text{tol}_\xi$	Lemma 11.2
$N_{ec,\mathcal{P}}$	$N_{ec,\mathcal{P}} := \bigcup_{\xi \in \mathcal{P}} \{\xi_i, i = 1, \dots, n_\xi\}$	eq. (11.2)
\mathcal{C}	measure for the \mathcal{P} -connectivity of the domain decomposition	eq. (11.3)

98 about the implementation due to the encounter of singular matrices for certain ex-
 99 tension operators described in section 9. Finally, in section 14, we present numerical
 100 results for a selection of coefficient functions.

101 For the reader's convenience, an overview of some definitions is given in Table 1.
 102

103 **2. Linear elasticity.** We will consider a variational formulation of the equa-
 104 tions of compressible linear elasticity: Find $u \in (H_0^1(\Omega))^3$ such that

$$105 \quad (2.1) \quad a_\Omega(u, v) = L(v) \quad \forall v \in (H_0^1(\Omega))^3,$$

106 where $\Omega \subset \mathbb{R}^3$ is a polyhedral domain and

$$107 \quad a_\Omega(u, v) := \int_\Omega 2\mu(x) \left(\varepsilon(u(x)) : \varepsilon(v(x)) \right) dx + \int_\Omega \lambda(x) \left(\text{div}(u(x)) \text{div}(v(x)) \right) dx,$$

$$108 \quad L(v) := \int_\Omega f(x) \cdot v(x) dx.$$

110 The Lamé parameters $0 < \lambda(x)$, $\mu(x) : \mathbb{R}^3 \rightarrow \mathbb{R}$ are scalar coefficient functions,
 111 $f \in (L^2(\Omega))^3$,

$$112 \quad \varepsilon(u) := \frac{1}{2} \left(\nabla u + (\nabla u)^T \right)$$

113 and

$$114 \quad A : B := \text{tr}(A^T B) = \sum_{i,j=1}^d A_{ij} B_{ij}.$$

115 for any matrices $A, B \in \mathbb{R}^{3 \times 3}$.

116 We will consider problems with a highly heterogeneous Young modulus $E: \Omega \rightarrow$
 117 \mathbb{R} , $0 < E_{\min} \leq E(x) \leq E_{\max}$, and a positive Poisson ratio ν , bounded away, from
 118 above, by $1/2$, and we define the Lamé parameters by

$$119 \quad \lambda(x) := \frac{E(x)\nu}{(1+\nu)(1-2\nu)},$$

$$120 \quad \mu(x) := \frac{E(x)}{2(1+\nu)}.$$

122 The algorithms described in this paper can also be applied to other linear,
 123 second-order elliptic problems including those in two dimensions.

124 Let $\tau_h := \tau_h(\Omega)$ be a finite element discretization of Ω . We will use a conforming
 125 space $V^h(\Omega)$ of piecewise linear or trilinear finite elements on this mesh, and for
 126 simplicity assume that the Lamé parameters are constant on each element $T \in \tau_h$.

127 We will use the conjugate gradient method preconditioned by two-level over-
 128 lapping Schwarz methods to solve the resulting linear system $Ku = b$.

129 For completeness, we note that the Dirichlet boundary condition has been in-
 130 corporated into the global stiffness matrix by setting those rows and columns of K
 131 to unit vectors that correspond to Dirichlet boundary nodes.

132 **3. Two-level overlapping Schwarz methods.** We will now introduce the
 133 two-level Schwarz algorithms, mostly following [43, Chapter 2.2]. The different
 134 variants considered in this paper will differ in the coarse space chosen; the design of
 135 the coarse space is the main issue in this study and many other studies of algorithms
 136 of this kind. In the next five sections, we will introduce four different variants. In
 137 [section 12](#), we also explore alternatives that decrease the costs of using the two
 138 algorithms which use adaptive choices of their coarse spaces.

139 We partition the domain Ω into N nonoverlapping subdomains Ω_i with a max-
 140 imum diameter H , each a union of finite elements, and denote the corresponding
 141 interface by $\Gamma := \bigcup_{i \neq j} (\partial\Omega_i \cap \partial\Omega_j) \setminus \partial\Omega$. We extend each subdomain Ω_i by k lay-
 142 ers of finite elements to obtain an overlapping domain decomposition $\{\Omega'_i\}_{i=1}^N$ and
 143 introduce subspaces $V_i := V^h(\Omega'_i)$, $i \in 1, \dots, N$, of finite element functions that
 144 vanish on $\partial\Omega'_i$ and in the complement of Ω'_i .

145 Associated with each such subdomain is a restriction operator $R_i: V^h(\Omega) \rightarrow V_i$
 146 and an extension operator $R_i^T: V_i \rightarrow V^h$. Furthermore, for any global coarse space
 147 $V_0 \subset V^h$, we define a linear interpolation operator $R_0: V^h \rightarrow V_0$, where each of
 148 the columns of the matrix R_0^T represents a coarse basis function defined on the fine
 149 mesh τ_h .

150 We will use exact solvers for all the subspaces defined in terms of bilinear forms
 151 on V_i , $i \in \{0, 1, \dots, N\}$, given by

$$152 \quad \tilde{a}_i(u_i, v_i) = a_\Omega(R_i^T u_i, R_i^T v_i) \quad \forall u_i, v_i \in V_i;$$

154 cf. [43, Chapter 2.2]. The associated matrices are given by $K_i = R_i K R_i^T$, $i =$
 155 $0, 1, \dots, N$. The additive one-level Schwarz preconditioned operator is given by
 156 $P_{\text{OS-1}} = \sum_{i=1}^N R_i^T K_i^{-1} R_i K$, and that of the additive two-level Schwarz operator by

$$157 \quad P_{\text{OS-2}} = R_0^T K_0^{-1} R_0 K + P_{\text{OS-1}}.$$

158 **4. The GDSW preconditioner.** In what follows, x^h will denote a finite
 159 element node. Those on the interface form the set $\Gamma^h := \{x^h \in \Gamma\}$. A key ingredient
 160 of each of our coarse spaces is a partition \mathcal{P} of Γ^h into disjoint interface components
 161 $\xi^h \subset \Gamma^h$, s.t.

$$162 \quad \Gamma^h = \bigcup_{\xi^h \in \mathcal{P}} \xi^h.$$

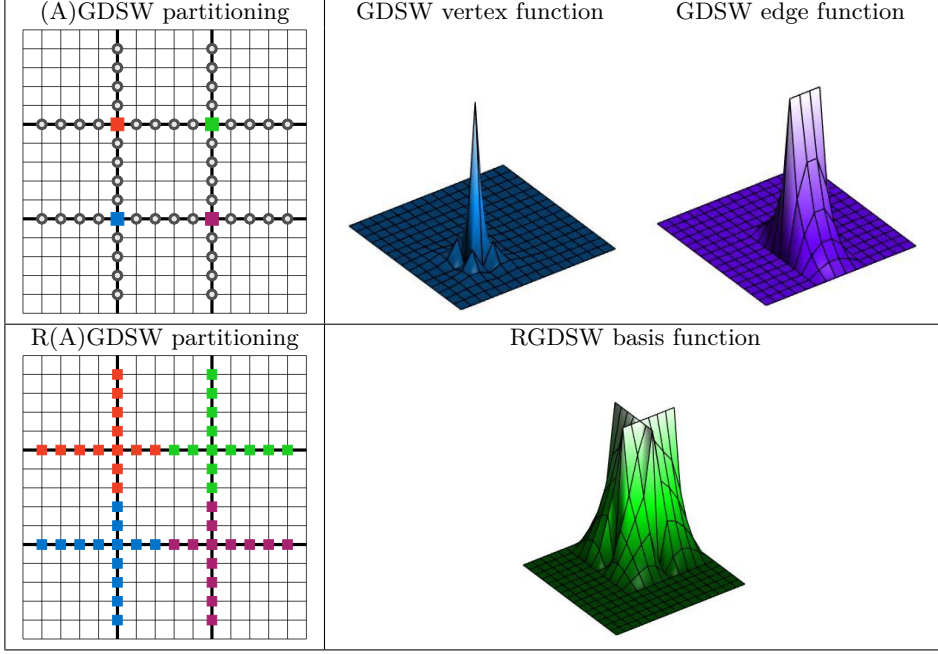


FIG. 1. **Left:** Decomposition of the interface Γ^h . **Top-Left:** Decomposition of Γ^h into 16 components: 4 vertices and 12 edges (with 4 nodes each) as used in the GDSW and adaptive GDSW method. **Bottom-Left:** Decomposition of Γ^h into 4 components as used in the reduced dimension GDSW and reduced dimension adaptive GDSW methods. **Right:** Corresponding coarse functions for a two-dimensional diffusion problem are shown on the right for GDSW (top) and RGDSW (bottom). Homogeneous Dirichlet boundary conditions are assumed on $\partial\Omega$. The GDSW vertex function (top-center) corresponds to the blue vertex. The GDSW edge function (top-right) corresponds to the edge between the blue and magenta vertices. The RGDSW coarse function (bottom-right) corresponds to the green component.

163 To simplify, we will omit the superscript h and write ξ instead of ξ^h .

164 The GDSW, [5, 6], AGDSW, [19, 21], RGDSW, [9, 27] and section 6, and
 165 RAGDSW, section 7, preconditioners are two-level overlapping Schwarz methods,
 166 and their preconditioners can be written in matrix form as

$$167 \quad M^{-1} = \Phi (\Phi^T K \Phi)^{-1} \Phi^T + \sum_{i=1}^N R_i^T K_i^{-1} R_i.$$

168 The basis functions of all our coarse spaces, i.e., the columns of Φ , are defined by an
 169 energy-minimal extension of the values Φ_Γ on the interface Γ^h to the subdomains,
 170 i.e., by

$$171 \quad \Phi = \begin{bmatrix} \Phi_I \\ \Phi_\Gamma \end{bmatrix} = H_\Gamma \Phi_\Gamma, \quad H_\Gamma := \begin{bmatrix} -K_{II}^{-1} K_{I\Gamma} \\ I_\Gamma \end{bmatrix}.$$

172 Here I_Γ is the identity matrix on Γ^h and H_Γ is constructed from submatrices of the
 173 global stiffness matrix

$$174 \quad K := \begin{bmatrix} K_{II} & K_{I\Gamma} \\ K_{\Gamma I} & K_{\Gamma\Gamma} \end{bmatrix},$$

175 where I refers to the set of variables not associated with the interface. We note
 176 that I also contains boundary nodes of Ω . We note that K_{II} is block-diagonal and

177 that $K_{\Gamma I} = K_{II}^T$ also can be written in block form as

$$178 \quad K_{II} = \begin{bmatrix} K_{II}^{(1)} & & \\ & \ddots & \\ & & K_{II}^{(N)} \end{bmatrix}, K_{\Gamma I} = \begin{bmatrix} K_{\Gamma I}^{(1)} & \dots & K_{\Gamma I}^{(N)} \end{bmatrix}.$$

179 The superscripts of these matrices mark contributions from the subdomains Ω_i to
180 the stiffness matrix K .

181 Given the sparsity of the stiffness matrix, reflecting the local coupling of the
182 variables, all these matrix blocks are sparse and the coarse space basis functions
183 are each associated only with a few subdomains. In the original GDSW method for
184 the scalar two-dimensional case, the columns of Φ_Γ are given by the characteristic
185 functions of vertices and subdomain edges, i.e., the interface is partitioned as follows:
186 $\Gamma^h = (\bigcup_{v \in \mathcal{V}} v) \cup (\bigcup_{e \in \mathcal{E}} e)$, where \mathcal{V} and \mathcal{E} are the sets of subdomain vertices
187 and edges, respectively, cf. [Figure 1](#) (top-left) for the interface partition and (top-
188 right) for two corresponding coarse functions. For the three dimensional case, the
189 basis functions are defined analogously, using characteristic functions for interface
190 vertices, edges, and faces.

191 In more general cases, the boundary values on Γ span the restriction of the null
192 space of K^N to Γ , where K^N is the stiffness matrix given by $a_\Omega(\cdot, \cdot)$ with a Neumann
193 boundary condition on $\partial\Omega$. Thus, for linear elasticity in three dimensions, and any
194 subdomain edge which is not straight, we obtain 6 functions: 3 translations and 3
195 rotations. We note that the restriction of the rigid body modes to a straight edge
196 are linear dependent; see [\[7\]](#).

197 The matrix of the GDSW coarse operator can be computed either by forming
198 the triple matrix product

$$199 \quad \Phi^T K \Phi$$

200 or by exploiting the fact that

$$201 \quad \Phi^T K \Phi = \begin{bmatrix} -K_{II}^{-1} K_{I\Gamma} \Phi_\Gamma \\ \Phi_\Gamma \end{bmatrix}^T \begin{bmatrix} K_{II} & K_{I\Gamma} \\ K_{\Gamma I} & K_{\Gamma\Gamma} \end{bmatrix} \begin{bmatrix} -K_{II}^{-1} K_{I\Gamma} \Phi_\Gamma \\ \Phi_\Gamma \end{bmatrix}$$

$$202 \quad = \Phi_\Gamma^T S_{\Gamma\Gamma} \Phi_\Gamma,$$

204 where $S_{\Gamma\Gamma} = K_{\Gamma\Gamma} - K_{\Gamma I} K_{II}^{-1} K_{I\Gamma}$ is the Schur complement obtained by eliminating
205 the interior variables of all subdomains and those on the boundary of Ω .

206 **5. Standard adaptive GDSW coarse space.** The standard adaptive
207 GDSW method, the AGDSW method, uses the same interface partitioning \mathcal{P} , based
208 on subdomain vertices, edges, and faces, as the GDSW method. The coarse func-
209 tions for the vertices are the same as for the GDSW variant but the columns of Φ
210 corresponding to the edges and faces are not. Instead, we use a few of the eigen-
211 functions of local generalized eigenvalue problems of the form

$$212 \quad (5.1) \quad S_{\xi\xi} \tau_{*,\xi} = \lambda_{*,\xi} K_{\xi\xi}^{\Omega_\xi} \tau_{*,\xi},$$

213 where ξ corresponds to an edge or a face.

214 To define the Schur complement $S_{\xi\xi}$ and the matrix $K_{\xi\xi}^{\Omega_\xi}$, for any edge and
215 face ξ , we will use the local stiffness matrix K^{Ω_ξ} on Ω_ξ with Neumann boundary
216 conditions. Here $\bar{\Omega}_\xi$ is the closure of the union of all subdomains which are adjacent
217 to ξ and $\Omega_\xi := \bar{\Omega}_\xi \setminus \partial\Omega_\xi$ its interior. The stiffness matrix K^{Ω_ξ} is defined by $a_{\Omega_\xi}(\cdot, \cdot)$
218 and can be assembled from the subdomain stiffness matrices of the subdomains
219 adjacent to the edge or face.

220 We partition the degrees of freedom of Ω_ξ into the set associated with ξ and
 221 the rest which forms a set R and write the stiffness matrix as

$$222 \quad K^{\Omega_\xi} = \begin{pmatrix} K_{RR}^{\Omega_\xi} & K_{R\xi}^{\Omega_\xi} \\ K_{\xi R}^{\Omega_\xi} & K_{\xi\xi}^{\Omega_\xi} \end{pmatrix}.$$

223 and can then define the Schur complement by

$$224 \quad S_{\xi\xi} := K_{\xi\xi}^{\Omega_\xi} - K_{\xi R}^{\Omega_\xi} \left(K_{RR}^{\Omega_\xi} \right)^+ K_{R\xi}^{\Omega_\xi},$$

225 where $\left(K_{RR}^{\Omega_\xi} \right)^+$ is a pseudoinverse of $K_{RR}^{\Omega_\xi}$; see [Remark 9.1](#) and [section 13](#).

226 We sort the eigenvalues of (5.1) in nondecreasing order; i.e., $\lambda_{1,\xi} \leq \lambda_{2,\xi} \leq \dots \leq$
 227 $\lambda_{m,\xi}$ where m is the number of unknowns of (5.1). We select all eigenvectors $\tau_{*,\xi}$,
 228 with eigenvalues smaller or equal than a certain threshold, i.e., $\lambda_{*,\xi} \leq \text{tol}_\xi$ and then
 229 define $\tau_{*,\Gamma}$ as the extension by zero of $\tau_{*,\xi}$ from ξ to Γ^h . The coarse basis functions
 230 corresponding to ξ are then the extensions

$$231 \quad v_{*,\xi} := H_\Gamma \tau_{*,\Gamma}$$

232 and the columns of Φ are now given by the $v_{*,\xi}$, selected, and the GDSW vertex
 233 functions.

234 Let $\text{tol}_\mathcal{E}$ and $\text{tol}_\mathcal{F}$ be the smallest tolerance used for the subdomain edges and
 235 faces, respectively. The following condition number estimate for the preconditioned
 236 operator has been derived previously for scalar diffusion problems; see [[21](#), [Corol-](#)
 237 [lary 6.6](#)]:

238 **LEMMA 5.1.** *The condition number of the AGDSW two-level Schwarz operator*
 239 *in three dimensions is bounded by*

$$240 \quad \kappa(M_{\text{AGDSW}}^{-1}K) \leq \left(20 + \frac{34(N^\mathcal{E})^2 n_{\max}^\mathcal{E}}{\text{tol}_\mathcal{E}} + \frac{68(N^\mathcal{F})^2}{\text{tol}_\mathcal{F}} \right) (\hat{N}_c + 1).$$

241 *The constant \hat{N}_c is an upper bound of the number of overlapping subdomains that*
 242 *any point $x^h \in \Omega$ can belong to. $N^\mathcal{E}$ and $N^\mathcal{F}$ are the maximum number of subdomain*
 243 *edges and faces, respectively, of any subdomain. $n_{\max}^\mathcal{E}$ is the maximum number of*
 244 *subdomains that share a subdomain edge. All constants are independent of H , h ,*
 245 *and the contrast of the coefficient function.*

246 This kind of result also holds for linear elasticity; see [Corollary 11.5](#) and [section 11](#).

247 **Remark 5.2.** If $\text{tol}_\xi = 0$ for all $\xi \in \mathcal{P}$, the AGDSW coarse space contains only
 248 the coarse functions of the GDSW coarse space. Thus, we obtain

$$249 \quad V_{\text{GDSW}} = V_{\text{AGDSW}}^0 \subset V_{\text{AGDSW}}^{\text{tol}(\mathcal{P})};$$

250 cf. also [Remark 7.1](#).

251 **6. A reduced dimension GDSW coarse space.** We will first give a simple
 252 description of an interface partition for a structured mesh and domain decomposition.
 253 This partition can also be used for the reduced dimension adaptive GDSW
 254 coarse spaces.

255 Our goal is to reduce the number of interface components. To this end, each
 256 vertex of the coarse mesh will be associated with an interface component ξ formed by
 257 parts of the edges and faces adjacent to the vertex. A disjoint partition is obtained
 258 by distributing parts of these faces and edges equally, or almost equally, between
 259 nearby vertices; see [Figure 1](#) (bottom-left) for a two-dimensional representation.

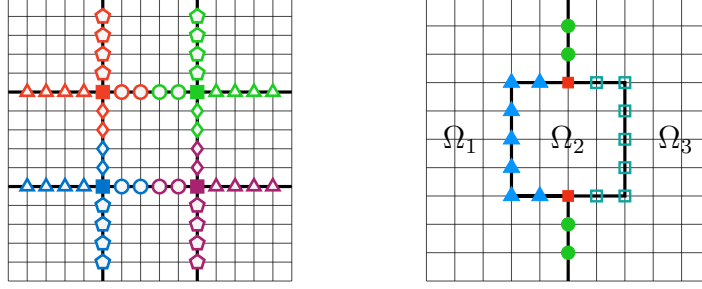


FIG. 2. **Left:** Partitioning of the RGDSW interface components into the respective parts of vertices and edges as required for the right hand side of the generalized eigenvalue problem in the RAGDSW method. Each component is partitioned into 5 subcomponents (4 edges, 1 vertex). **Right:** The image shows a case, in which a NEC can consist of two disjoint connected components. The interface of the domain $\Omega = \cup_{i=1}^3 \Omega_i$ is indicated by thick black lines.

260 The reduced dimension GDSW coarse space is then defined completely analo-
 261 gously to the GDSW coarse space. Thus the restriction of the null space elements
 262 to the interface components is first extended by zero to the rest of the interface
 263 nodes and then extended with minimal energy to the subdomain interiors to obtain
 264 the coarse functions; see Figure 1 (bottom-right) for one of the coarse functions for
 265 a two-dimensional diffusion problem.

266 We note that our RGDSW coarse space differs from those of [9] but that can
 267 be regarded as a variant of the coarse spaces introduced in that paper.

268 **7. The reduced dimension adaptive GDSW coarse space.** For the re-
 269 duced adaptive GDSW coarse space, we need to partition each interface component
 270 ξ , as those of the previous section, into subcomponents. For a structured mesh and
 271 domain decomposition, as in that section, we partition each ξ into subsets related to
 272 the subdomain vertices, edges, and faces. With \mathcal{V} , \mathcal{E} , and \mathcal{F} the sets of subdomain
 273 vertices, edges, and faces, respectively, we define subcomponents ξ_i of ξ such that

$$274 \quad (7.1) \quad \{\xi_i\}_{i=1}^{n_\xi} = \{\xi \cap c : c \in \mathcal{V} \cup \mathcal{E} \cup \mathcal{F} \wedge c \cap \xi \neq \emptyset\},$$

275 where n_ξ is the number of subcomponents of ξ ; see Figure 2 (left) for a two-
 276 dimensional case. We next partition $K_{\xi\xi}^{\Omega_\xi}$ with respect to the subsets $\{\xi_i\}_{i=1}^{n_\xi}$, into

$$277 \quad K_{\xi\xi}^{\Omega_\xi} = \left(K_{\xi_i\xi_j}^{\Omega_\xi} \right)_{i,j=1}^{n_\xi}$$

278 and, as before, we define the Schur complement by

$$279 \quad S_{\xi\xi} := K_{\xi\xi}^{\Omega_\xi} - K_{\xi R}^{\Omega_\xi} \left(K_{RR}^{\Omega_\xi} \right)^+ K_{R\xi}^{\Omega_\xi},$$

280 where $\left(K_{RR}^{\Omega_\xi} \right)^+$ is a pseudoinverse of $K_{RR}^{\Omega_\xi}$; see Remark 9.1 and section 13. Fur-
 281 thermore, let

$$282 \quad (7.2) \quad \tilde{K}_{\xi\xi} := \text{blockdiag} \left(K_{\xi_i\xi_i}^{\Omega_\xi} \right)_{i=1, \dots, n_\xi}$$

283 and introduce a generalized eigenvalue problem, given in matrix form by

$$284 \quad S_{\xi\xi} \tau_{*,\xi} = \lambda_{*,\xi} \tilde{K}_{\xi\xi} \tau_{*,\xi}.$$

285 As in section 5, the eigenvalues are sorted in a nondecreasing order and eigen-
 286 vectors $\tau_{*,\xi}$ corresponding to $\lambda_{*,\xi} \leq \text{tol}_\xi$ are selected and then extended by zero to
 287 Γ^h as $\tau_{*,\Gamma}$. The coarse basis functions, i.e., the columns of Φ , corresponding to ξ
 288 are the extensions $v_{*,\xi} := H_\Gamma \tau_{*,\Gamma}$.

289 *Remark 7.1.* If $tol_\xi = 0$ for all $\xi \in \mathcal{P}$, the RAGDSW coarse space contains only
 290 the coarse functions associated with the null space of the Schur complement $S_{\xi\xi}$.
 291 The latter is identical to the null space of K^{Ω_ξ} restricted to ξ . Thus, in this case,
 292 RAGDSW reduces to RGDSW, and we have

$$293 \quad V_{\text{RGDSW}} = V_{\text{RAGDSW}}^0 \subset V_{\text{RAGDSW}}^{\text{tol}(\mathcal{P})}$$

294 **8. Interface partitioning for RAGDSW on unstructured meshes.** For
 295 unstructured cases, we will define the partitioning \mathcal{P} using nodal equivalence classes
 296 and begin with definitions of connected components of finite element nodes and of
 297 nodal equivalence classes. We note that equivalence classes have previously been
 298 used in [9] for similar purposes.

299 Two finite element nodes $x_1^h, x_2^h \in \Gamma^h$ are said to be adjacent, if there exists
 300 a finite element edge or face $z \subset \Gamma$ such that $x_1^h, x_2^h \in \bar{z}$, the closure of z . A set
 301 of nodes $\gamma \subset \Gamma^h$ is said to form a connected component, if, for any two nodes
 302 $x_0^h, x_s^h \in \gamma$, there exists a path (x_0^h, \dots, x_s^h) , $x_i^h \in \gamma$, of adjacent nodes.

303 For any node $x^h \in \Omega$, let

$$304 \quad (8.1) \quad n(x^h) := \{i \in \{1, 2, \dots, N\} : x^h \in \bar{\Omega}_i\}$$

305 be the set of indices of the subdomains which have x^h in common. To partition
 306 a set of nodes $\gamma \subset \Gamma^h$, we define nodal equivalence classes (NECs) by the relation
 307 $x_1^h \sim x_2^h \Leftrightarrow n(x_1^h) = n(x_2^h)$, for any two nodes $x_1^h, x_2^h \in \gamma$. We further partition each
 308 NEC into its connected components based on the adjacency of nodes; cf. [Figure 2](#)
 309 (right).

310 By $\mathcal{N}(x^h)$, we denote the NEC of a node $x^h \in \gamma$, i.e., $x^h \in \mathcal{N}(x^h)$. If $n(x_2^h) \subsetneq$
 311 $n(x_1^h)$, then $\mathcal{N}(x_1^h)$ is said to be an ancestor of $\mathcal{N}(x_2^h)$ which in turn is a descendant
 312 of $\mathcal{N}(x_1^h)$. If a NEC does not have an ancestor, we call it a root.

313 We note that for $\gamma = \Gamma^h$ a root is a vertex (i.e., a coarse node) in the case
 314 of cuboid subdomains. However, often for unstructured domain decompositions
 315 obtained, e.g., by METIS [29], a root can be a coarse edge or coarse face as well; see
 316 further the discussion in [9]. We note that for special cases of structured domain
 317 decompositions, e.g., a beam built from a union of cubes, the same can occur.

318 We now give a general description of the interface partition for RAGDSW for
 319 an unstructured mesh and domain decomposition. We will define components ξ ,
 320 s.t. each ξ contains only one root and parts of its descendants. Furthermore, we
 321 will assure that the resulting interface partition \mathcal{P} is nonoverlapping to obtain a
 322 partition \mathcal{P} of connected disjoint components $\xi \in \mathcal{P}$ s.t.

$$323 \quad \Gamma^h = \bigcup_{\xi \in \mathcal{P}} \xi.$$

324 Several specific constructions are possible. Relevant aspects are, e.g., obtaining
 325 components of similar size, nondegenerate components, and parallel efficiency of
 326 the construction.

327 For the results in this paper, we have constructed the interface partition in the
 328 following way: We initialize each component $\xi \in \mathcal{P}$ with the nodes of a root and
 329 add the remaining nodes in an iterative process.

330 Starting with the roots, we grow sets which will result in all the subsets $\xi \in \mathcal{P}$.
 331 In each step of an iteration, we add all nodes which are adjacent to elements of
 332 each of the current sets, which have not been previously assigned, and which are
 333 descendants of the root of the set. We repeat this process until all interface nodes
 334 have been assigned to a $\xi \in \mathcal{P}$. [Figure 3](#) depicts sample partitions for two and three
 335 dimensions.

336 We note that for the unstructured meshes in [section 14](#), the average number of
 337 degrees of freedom per eigenvalue problem is increased by roughly 50% and with

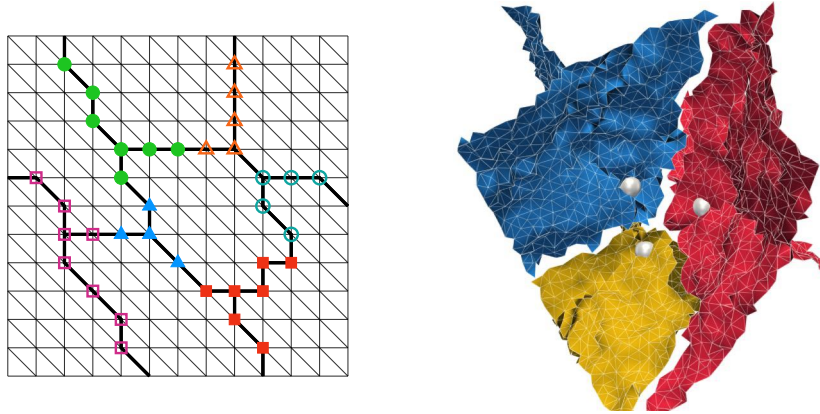


FIG. 3. Sample partitions in two dimensions (*left*) and three dimensions (*right*) for unstructured domain decompositions. For the two-dimensional case, the interface is given by thick black lines and the interface components $\xi \in \mathcal{P}$ by different markers. For the three-dimensional case, coarse nodes are indicated by white spheres; interface components are shown in different colors. For a clearer visualization, only those finite element faces are shown, whose nodes are all contained in the respective interface component. Thus, gaps indicate finite element faces, whose nodes are part of several interface components.

338 the maximum roughly doubled, compared to the face eigenvalue problems used in
 339 the standard AGDSW.

340 As before, we partition each interface component into its subcomponents. Let
 341 \mathcal{N}_{Γ^h} be the set of NECs of Γ^h and for $\xi \in \mathcal{P}$ let

$$342 \quad \mathcal{N}_\xi := \{\xi \cap c : c \in \mathcal{N}_{\Gamma^h} \wedge \xi \cap c \neq \emptyset\}.$$

343 Let $n_\xi := |\mathcal{N}_\xi|$ be the number of NECs of ξ and let ξ_i , $i = 1, \dots, n_\xi$, be the
 344 resulting decomposition of ξ into $\{\xi_i\}_{i=1}^{n_\xi} = \mathcal{N}_\xi$. We then have $\xi_i \cap \xi_j = \emptyset$ ($i \neq j$)
 345 and $\xi = \bigcup_{i=1}^{n_\xi} \xi_i$.

346 *Remark 8.1.* If our problem satisfies a Neumann boundary condition on $\partial\Omega_N \subset$
 347 $\partial\Omega$, in addition to a nonempty set $\partial\Omega_D = \partial\Omega \setminus \partial\Omega_N$ with a Dirichlet boundary
 348 condition, then the construction of the RAGDSW coarse space and the proof of the
 349 condition number estimate in sections 10 and 11 will essentially be the same. The
 350 finite element nodes that lie on the Neumann boundary but not on the interface
 351 $\Gamma = \bigcup_{i \neq j} (\partial\Omega_i \cap \partial\Omega_j) \setminus \partial\Omega_D$ are treated as interior nodes.

352 In the next section, we will first describe the adaptive GDSW coarse spaces in
 353 variational form. Thereafter, we will derive a condition number estimate for the
 354 preconditioned two-level additive Schwarz operator based on the coarse space in-
 355 troduced above. We note that the proof remains valid for quite general interface
 356 partitions \mathcal{P} and is not restricted to the one of RAGDSW.

357 **9. Variational description of adaptive GDSW-type coarse spaces.** For
 358 $\xi \in \mathcal{P}$ the index set n^ξ contains the indices of all adjacent subdomains, i.e., the
 359 union of the index sets of all nodes $x^h \in \xi$,

$$360 \quad (9.1) \quad n^\xi = \bigcup_{x^h \in \xi} n(x^h).$$

361 As in section 5, $\bar{\Omega}_\xi$ is the closure of the union of adjacent subdomains, i.e., $\bar{\Omega}_\xi =$
 362 $\bigcup_{i \in n^\xi} \bar{\Omega}_i$.

363 Let $\bar{G} \subset \bar{\Omega}$ be any union of sets $s \in \{\bar{T}_i \cap \bar{T}_j \neq \emptyset : T_i, T_j \in \tau_h\}$. By $z_{\xi \rightarrow G}(\cdot)$, we

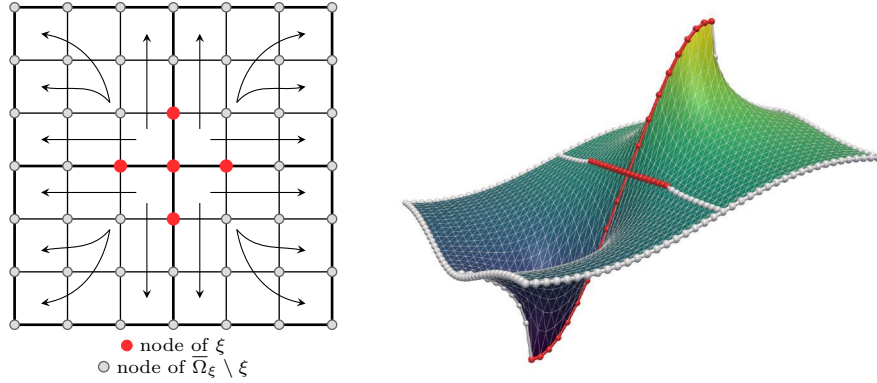


FIG. 4. Graphical representation in two dimensions of the energy-minimal extension (9.3) from $\xi \in \mathcal{P}$ to $\bar{\Omega}_\xi$ (left) and sample energy-minimal extension for the diffusion equation (right) in which the RAGDSW interface component ξ is highlighted in red and the remaining interface nodes in light gray.

364 denote an extension-by-zero operator from $\xi \subset G$ to G :

$$365 \quad (9.2) \quad \begin{aligned} z_{\xi \rightarrow G} : X^h(\xi) &\rightarrow \{w|_{\bar{G}} : w \in V^h(\Omega), w = 0 \text{ in } \bar{\Omega} \setminus \xi\} \\ v &\mapsto z_{\xi \rightarrow G}(v) := \begin{cases} v(x^h) & \forall x^h \in \xi, \\ 0 & \forall x^h \in \bar{G} \setminus \xi. \end{cases} \end{aligned}$$

366 Here, $X^h(\xi) := \{v : \xi \rightarrow \mathbb{R}^3\}$.

367 By $\mathcal{H}_{\xi \rightarrow \Omega_\xi}(\cdot)$, we denote a possibly nonunique (cf. Remark 9.1) energy-minimal
368 extension w.r.t. $a_{\Omega_\xi}(\cdot, \cdot)$ from ξ to $\bar{\Omega}_\xi$: let $V_{0,\xi}^h(\Omega_\xi) := \{w|_{\Omega_\xi} : w \in V^h(\Omega), w(x^h) =$
369 $0 \forall x^h \in \xi\}$, then for $\tau_\xi \in X^h(\xi)$, an extension $v_\xi := \mathcal{H}_{\xi \rightarrow \Omega_\xi}(\tau_\xi) \in V^h(\Omega_\xi)$ is given
370 by a solution of

$$371 \quad (9.3) \quad \begin{aligned} a_{\Omega_\xi}(v_\xi, v) &= 0 \quad \forall v \in V_{0,\xi}^h(\Omega_\xi), \\ v_\xi(x^h) &= \tau_\xi(x^h) \quad \forall x^h \in \xi; \end{aligned}$$

372 cf. Figure 4. We note that the extension is computed with a homogeneous Neumann
373 boundary condition on $\partial\Omega_\xi$.

374 As in section 8, let $\{\xi_i\}_{i=1}^{n_\xi}$ be the set of all NECs of a $\xi \in \mathcal{P}$. Then $\xi_i \cap \xi_j = \emptyset$
375 ($i \neq j$) and $\xi = \bigcup_{i=1}^{n_\xi} \xi_i$ holds. We define the symmetric, positive definite bilinear
376 form

$$377 \quad (9.4) \quad c_\xi(u, v) := \sum_{i=1}^{n_\xi} c_{\xi_i}(u, v) \quad \forall u, v \in X^h(\xi),$$

378 with

$$379 \quad (9.5) \quad c_{\xi_i}(u, v) := a_{\Omega_{\xi_i}}(z_{\xi_i \rightarrow \Omega_{\xi_i}}(u), z_{\xi_i \rightarrow \Omega_{\xi_i}}(v)) \quad \forall u, v \in X^h(\xi).$$

380 The corresponding norm is defined by

$$381 \quad (9.6) \quad \|u\|_{c_\xi}^2 := c_\xi(u, u) \quad \forall u \in X^h(\xi).$$

382 We define the following generalized eigenvalue problem on $\xi \in \mathcal{P}$: Find $\tau_{*,\xi} \in X^h(\xi)$
383 such that

$$384 \quad (9.7) \quad a_{\Omega_\xi}(\mathcal{H}_{\xi \rightarrow \Omega_\xi}(\tau_{*,\xi}), \mathcal{H}_{\xi \rightarrow \Omega_\xi}(\theta)) = \lambda_{*,\xi} c_\xi(\tau_{*,\xi}, \theta) \quad \forall \theta \in X^h(\xi).$$

386 The eigenvalues are again sorted in nondescending order; i.e., $\lambda_{1,\xi} \leq \lambda_{2,\xi} \leq \dots \leq$
 387 $\lambda_{m,\xi}$ and the eigenmodes accordingly, where $m = \dim(X^h(\xi))$. Furthermore, let
 388 the eigenmodes $\tau_{*,\xi}$ satisfy $c_\xi(\tau_{k,\xi}, \tau_{j,\xi}) = \delta_{kj}$, where δ_{kj} is the Kronecker delta
 389 symbol. We select all eigenmodes $\tau_{*,\xi}$ where the eigenvalues are below a certain
 390 threshold, i.e., $\lambda_{*,\xi} \leq \text{tol}_\xi$. Then, the coarse basis functions corresponding to ξ are
 391 the extensions

$$392 \quad (9.8) \quad v_{*,\xi} := \mathcal{H}_{\Gamma \rightarrow \Omega}(\tau_\Gamma) \in V_0^h(\Omega), \quad \tau_\Gamma := z_{\xi \rightarrow \Gamma}(\tau_{*,\xi}),$$

393 of the selected $\tau_{*,\xi}$, where $v_{*,\xi} = \mathcal{H}_{\Gamma \rightarrow \Omega}(\tau_\Gamma)$ is given by the solution $v_{*,\xi} \in V_0^h(\Omega)$
 394 that satisfies

$$395 \quad (9.9) \quad \begin{aligned} a_{\Omega_l}(v_{*,\xi}, w) &= 0 & \forall w \in V_0^h(\Omega_l), l = 1, \dots, N, \\ v_{*,\xi}(x^h) &= \tau_\Gamma(x^h) & \forall x^h \in \Gamma^h. \end{aligned}$$

396 We note that, contrary to (9.7), $v_{*,\xi}$ vanishes on $\partial\Omega_\xi$ since $\tau_\Gamma = z_{\xi \rightarrow \Gamma}(\tau_{*,\xi})$ and since
 397 $v_{*,\xi} = \mathcal{H}_{\Gamma \rightarrow \Omega}(\tau_\Gamma) \in V_0^h(\Omega)$. Therefore, (9.9) has a unique solution.

398 For a general interface partition \mathcal{P} , we define the adaptive GDSW coarse space
 399 as

$$400 \quad (9.10) \quad V_{\mathcal{P}} := \bigoplus_{\xi \in \mathcal{P}} \text{span} \{v_{k,\xi} : \lambda_{k,\xi} \leq \text{tol}_\xi\}.$$

401 The standard AGDSW coarse space (see [21]) is based on the partition

$$402 \quad \mathcal{P} := \mathcal{F} \cup \mathcal{E} \cup \mathcal{V}.$$

403 Since vertices, edges, and faces are NECs, we then have

$$404 \quad c_\xi(u, v) = a_{\Omega_\xi}(z_{\xi \rightarrow \Omega_\xi}(u), z_{\xi \rightarrow \Omega_\xi}(v))$$

405 if ξ is a vertex, an edge, or a face.

406 *Remark 9.1.* For the diffusion case the energy-minimal extension defined by
 407 (9.3) has a unique solution. If an interface component ξ is a straight edge or a vertex
 408 then 1 or 3 rotations, respectively, are in the null space of the extension operator
 409 for linear elasticity. However, as all solutions of (9.3) have the same energy, the
 410 choice of the particular solution does not influence the solution of the generalized
 411 eigenvalue problem (9.7): let $v_{*,\xi} = \mathcal{H}_{\xi \rightarrow \Omega_\xi}(\tau_{*,\xi})$ be a solution of (9.3). Then all
 412 solutions are given by $v_{*,\xi} + r$, where $r \in \text{range}(\mathcal{H}_{\xi \rightarrow \Omega_\xi}(0))$; for linear elasticity r
 413 is a rigid body mode. Since $r \in V_{0,\xi}^h(\Omega_\xi)$, we have $a_{\Omega_\xi}(r, \mathcal{H}_{\xi \rightarrow \Omega_\xi}(\theta)) = 0$ by the
 414 definition of $\mathcal{H}_{\xi \rightarrow \Omega_\xi}(\theta)$. Therefore, $v_{*,\xi} + r$ solves (9.3) and

$$415 \quad a_{\Omega_\xi}(v_{*,\xi} + r, \mathcal{H}_{\xi \rightarrow \Omega_\xi}(\theta)) = a_{\Omega_\xi}(v_{*,\xi}, \mathcal{H}_{\xi \rightarrow \Omega_\xi}(\theta)) \quad \forall \theta \in X^h(\xi).$$

416 As a consequence, any operator defined by (9.3) yields the same generalized eigen-
 417 value problem (9.7). In section 13, we will provide some remarks on how to find
 418 the solution of (9.3) when it is not unique.

419 *Remark 9.2.* We note that the left hand side of eigenvalue problem (9.7) is
 420 singular and its kernel contains the constant functions for the scalar diffusion case
 421 and the rigid body modes for linear elasticity. Therefore, the null space has a
 422 dimension of 1 for the scalar diffusion problem and at least 3 for linear elasticity.
 423 For a vertex (i.e., $\xi = v \in \mathcal{V}$) the problem has only one (scalar diffusion) and three
 424 (linear elasticity) degrees of freedom. Thus, in the latter case, the solution is given
 425 by the vertex basis functions of the GDSW coarse space, i.e., the three translations
 426 in case of linear elasticity; cf. [21] and [7].

427 **10. Spectral projections.** We will now consider the projections

$$428 \quad (10.1) \quad \Pi_{\mathcal{P}} w := \sum_{\xi \in \mathcal{P}} \Pi_{\xi} w, \quad \Pi_{\xi} w := \sum_{\lambda_{k,\xi} \leq \text{tol}_{\xi}} c_{\xi}(w, v_{k,\xi}) v_{k,\xi}$$

430 onto the space $V_{\mathcal{P}}$. Here, $v_{k,\xi}$ are the energy-minimal extensions of the eigenfunc-
431 tions determined by (9.8) and $\lambda_{k,\xi}$ the corresponding eigenvalues from (9.7). For
432 $\xi \in \mathcal{P}$, let $d_{\xi}: X^h(\xi) \times X^h(\xi) \rightarrow \mathbb{R}$ be the symmetric, positive semidefinite bilinear
433 form

$$434 \quad (10.2) \quad d_{\xi}(\cdot, \cdot) := a_{\Omega_{\xi}}(\mathcal{H}_{\xi \rightarrow \Omega_{\xi}}(\cdot), \mathcal{H}_{\xi \rightarrow \Omega_{\xi}}(\cdot)).$$

436 For any union $B \subset \bar{\Omega}$ of finite elements $T \in \tau_h$, let

$$437 \quad (10.3) \quad |v|_{a(B)} := \sqrt{a_B(v, v)} \quad \forall v \in V^h(\Omega).$$

439 We find that

$$440 \quad (10.4) \quad |v|_{d_{\xi}}^2 := d_{\xi}(v, v) = |\mathcal{H}_{\xi \rightarrow \Omega_{\xi}}(v)|_{a(\Omega_{\xi})}^2 \leq |v|_{a(\Omega_{\xi})}^2 \quad \forall v \in V^h(\Omega),$$

441 due to the energy-minimal property of the extension operator.

442 Using standard arguments of spectral theory, we obtain two important properties
443 of the projection Π_{ξ} , required for the proof of the condition number estimate in
444 section 11; cf., e.g., [21, Lemma 5.3] and [20, Lemma 4.1].

445 **LEMMA 10.1.** *Let the eigenpairs $\{(\tau_{k,\xi}, \lambda_{k,\xi})\}_{k=1}^{\dim(X^h(\xi))}$ from (9.7) be chosen
446 such that $c_{\xi}(\tau_{k,\xi}, \tau_{j,\xi}) = \delta_{kj}$ and such that the eigenpairs are sorted in nondescending
447 order w.r.t. the eigenvalues. Then the operator Π_{ξ} defines a projection which is
448 orthogonal with respect to the bilinear form $d_{\xi}(\cdot, \cdot)$ and therefore*

$$449 \quad |u|_{d_{\xi}}^2 = |\Pi_{\xi} u|_{d_{\xi}}^2 + |u - \Pi_{\xi} u|_{d_{\xi}}^2, \quad \forall u \in X^h(\xi).$$

450 In addition, we have, from spectral theory,

$$451 \quad \|u - \Pi_{\xi} u\|_{c_{\xi}}^2 \leq \frac{1}{\text{tol}_{\xi}} |u - \Pi_{\xi} u|_{d_{\xi}}^2.$$

453 The following lemma follows directly from Lemma 10.1; cf. [21, Lemma 2].

454 **LEMMA 10.2.** *For $\xi \in \mathcal{P}$ and $u \in V^h(\Omega)$ it holds that*

$$455 \quad \|u - \Pi_{\xi} u\|_{c_{\xi}}^2 \leq \frac{1}{\text{tol}_{\xi}} \sum_{k \in n^{\xi}} |u|_{a(\Omega_k)}^2.$$

456 *Proof.* We have

$$457 \quad \|u - \Pi_{\xi} u\|_{c_{\xi}}^2 \stackrel{\text{Lemma 10.1}}{\leq} \frac{1}{\text{tol}_{\xi}} |u - \Pi_{\xi} u|_{d_{\xi}}^2 \leq \frac{1}{\text{tol}_{\xi}} |u|_{d_{\xi}}^2$$

$$458 \quad \stackrel{(10.4)}{\leq} \frac{1}{\text{tol}_{\xi}} |u|_{a(\Omega_{\xi})}^2 = \frac{1}{\text{tol}_{\xi}} \sum_{k \in n^{\xi}} |u|_{a(\Omega_k)}^2.$$

459 \square

460 **11. Convergence analysis.** To prove a condition number estimate, we will
 461 prove the existence of a stable decomposition; cf. [43, Chapter 2]. We therefore
 462 define the coarse interpolation $I_0 := \Pi_{\mathcal{P}}$ as the projection onto the coarse space
 463 $V_0 := V_{\mathcal{P}}$; cf. (9.10) and (10.1). Thus the coarse component of the stable decompo-
 464 sition is defined as

$$465 \quad u_0 := I_0 u := \Pi_{\mathcal{P}} u.$$

466

467 LEMMA 11.1. For $\xi \in \mathcal{P}$ and $u \in V^h(\Omega)$, we have

$$468 \quad \|u - u_0\|_{c_{\xi}}^2 = c_{\xi}(u - u_0, u - u_0) \leq \frac{1}{\text{tol}_{\xi}} \sum_{k \in n^{\xi}} |u|_{a(\Omega_k)}^2.$$

469 *Proof.* We have

$$470 \quad \begin{aligned} 471 \quad \|u - u_0\|_{c_{\xi}}^2 &= \sum_{i=1}^{n_{\xi}} |z_{\xi_i \rightarrow \Omega_{\xi_i}}(u - \Pi_{\mathcal{P}} u)|_{a(\Omega_{\xi_i})}^2 \\ 472 &= \sum_{i=1}^{n_{\xi}} |z_{\xi_i \rightarrow \Omega_{\xi_i}}(u - \Pi_{\xi} u)|_{a(\Omega_{\xi_i})}^2 \\ 473 &= \|u - \Pi_{\xi} u\|_{c_{\xi}}^2 \\ 474 &\stackrel{\text{Lemma 10.2}}{\leq} \frac{1}{\text{tol}_{\xi}} \sum_{k \in n^{\xi}} |u|_{a(\Omega_k)}^2. \end{aligned}$$

475

□

476 Next, we derive an estimate for the energy of the coarse component.

477 LEMMA 11.2. It holds that

$$478 \quad |u_0|_{a(\Omega)}^2 \leq 2 |u|_{a(\Omega)}^2 + \frac{2C_{\tau}}{\text{tol}_{\mathcal{P}}} \sum_{\xi \in \mathcal{P}} \sum_{k \in n^{\xi}} |u|_{a(\Omega_k)}^2 \leq 2 \left(1 + \frac{C_{\tau} N^{\xi}}{\text{tol}_{\mathcal{P}}} \right) |u|_{a(\Omega)}^2,$$

479

480 where C_{τ} is the maximum number of vertices of any element $T \in \tau_h(\Omega)$, and

$$481 \quad (11.1) \quad N^{\xi} := \max_{1 \leq i \leq N} |\mathcal{P}(\Omega_i)|, \quad \mathcal{P}(\Omega_i) := \{\xi \in \mathcal{P} : \xi \cap \bar{\Omega}_i \neq \emptyset\}$$

482 is the maximum number of interface components $\xi \in \mathcal{P}$ of any subdomain, and
 483 $\text{tol}_{\mathcal{P}} := \min_{\xi \in \mathcal{P}} \text{tol}_{\xi}$.

484 *Proof.* We can use the fact that u_0 is energy-minimal w.r.t. $|\cdot|_{a, \Omega_i}$ for each
 485 subdomain Ω_i , i.e., $u_0 = \mathcal{H}_{\Gamma \rightarrow \Omega}(u_0)$, and obtain

$$486 \quad \begin{aligned} |u_0|_{a(\Omega)}^2 &\leq 2 |\mathcal{H}_{\Gamma \rightarrow \Omega}(u)|_{a(\Omega)}^2 + 2 |\mathcal{H}_{\Gamma \rightarrow \Omega}(u - u_0)|_{a(\Omega)}^2 \\ 487 &\leq 2 |u|_{a(\Omega)}^2 + 2 |z_{\Gamma \rightarrow \Omega}(u - u_0)|_{a(\Omega)}^2. \end{aligned}$$

488

489 Let

$$490 \quad (11.2) \quad \mathcal{N}_{ec, \mathcal{P}} := \bigcup_{\xi \in \mathcal{P}} \{\xi_i, i = 1, \dots, n_{\xi}\}$$

491 be the set of interface components of the $\xi \in \mathcal{P}$ partitioned into their nodal equiv-
 492 alence classes ξ_i , $i = 1, \dots, n_{\xi}$. Then, $\xi_i \cap \xi_j = \emptyset$ for $i \neq j$, and $\bigcup_{\xi_i \in \mathcal{N}_{ec, \mathcal{P}}} \xi_i = \Gamma^h$,
 493 and

$$494 \quad \begin{aligned} |z_{\Gamma \rightarrow \Omega}(u - u_0)|_{a(\Omega)}^2 &= \left| \sum_{\xi_i \in \mathcal{N}_{ec, \mathcal{P}}} z_{\xi_i \rightarrow \Omega}(u - u_0) \right|_{a(\Omega)}^2 \\ 495 &= \sum_{T \in \tau_h(\Omega)} \left| \sum_{\xi_i \in \mathcal{N}_{ec, \mathcal{P}}} z_{\xi_i \rightarrow \Omega}(u - u_0) \right|_{a(T)}^2. \end{aligned}$$

496

497 There can be at most C_τ NECs ξ_i that are nonzero in any element T . Thus, we
 498 have using the Cauchy–Schwarz inequality

$$\begin{aligned}
 499 \quad \sum_{T \in \tau_h(\Omega)} \left| \sum_{\xi_i \in \mathcal{N}_{ec, \mathcal{P}}} z_{\xi_i \rightarrow \Omega} (u - u_0) \right|_{a(T)}^2 &\leq \sum_{T \in \tau_h(\Omega)} C_\tau \sum_{\xi_i \in \mathcal{N}_{ec, \mathcal{P}}} |z_{\xi_i \rightarrow \Omega} (u - u_0)|_{a(T)}^2 \\
 500 &= C_\tau \sum_{\xi_i \in \mathcal{N}_{ec, \mathcal{P}}} |z_{\xi_i \rightarrow \Omega} (u - u_0)|_{a(\Omega_{\xi_i})}^2 \\
 501 &= C_\tau \sum_{\xi \in \mathcal{P}} \|u - u_0\|_{c_\xi}^2 \\
 502 &\leq \frac{C_\tau}{\text{tol}_{\mathcal{P}}} \sum_{\xi \in \mathcal{P}} \sum_{k \in n^\xi} |u|_{a(\Omega_k)}^2, \\
 503
 \end{aligned}$$

504 where in the last step we have used [Lemma 11.1](#). Thus,

$$505 \quad |u_0|_{a(\Omega)}^2 \leq 2|u|_{a(\Omega)}^2 + 2 \frac{C_\tau}{\text{tol}_{\mathcal{P}}} \sum_{\xi \in \mathcal{P}} \sum_{k \in n^\xi} |u|_{a(\Omega_k)}^2 \leq 2 \left(1 + \frac{C_\tau N^\xi}{\text{tol}_{\mathcal{P}}} \right) |u|_{a(\Omega)}^2.$$

506

□

507 In [Theorem 11.4](#), we will derive estimates based on the product of $u - u_0$
 508 and a partition of unity function θ_i associated with each subdomain. We employ an
 509 overlapping decomposition $\{\tilde{\Omega}_i\}_{i=1}^N$ with overlap h by extending the nonoverlapping
 510 decomposition $\{\Omega_i\}_{i=1}^N$ by one layer of finite elements. The estimates are carried
 511 out separately on $\tilde{\Omega}_i \setminus \Omega_i$ and Ω_i : the former locally and the latter globally. The
 512 following lemma covers both cases.

513 **LEMMA 11.3.** *Let $l \in \{0, 1, \dots, N\}$ and $B = \tilde{\Omega}_l \setminus \Omega_l$, if $l > 0$, and $B = \Omega_0 := \Omega$
 514 for $l = 0$. Furthermore, let $\Psi : \bar{B} \rightarrow \mathbb{R}$ s.t. $\Psi|_{\xi_i}$ is constant on $\xi_i \in \mathcal{N}_{ec, \mathcal{P}}$, $\xi_i \subset \bar{B}$,
 515 i.e., $\Psi(x^h) = C_i$ for all $x^h \in \xi_i$. Additionally, we assume that $0 \leq \Psi \leq 1$ and
 516 $\Psi(x^h) = 0$ for $x^h \notin \Gamma^h \cap \bar{B}$. Then,*

$$517 \quad |I^h(\Psi \cdot (u - u_0))|_{a(B)}^2 \leq \frac{C_\tau}{\text{tol}_{\mathcal{P}}} \sum_{\xi \in \mathcal{P}(\Omega_l)} \sum_{k \in n^\xi} |u|_{a(\Omega_k)}^2,$$

518 where $I^h(\cdot)$ is the pointwise interpolation operator of the finite element space $V^h(\Omega)$.

519 *Proof.* We define the set $\mathcal{N}_{ec, \mathcal{P}}(\Omega_l) := \{\xi_j \in \mathcal{N}_{ec, \mathcal{P}} : \xi_j \cap \bar{\Omega}_l \neq \emptyset\}$ of NECs that
 520 are part of or touch Ω_l . Given that $\mathcal{P}(\Omega_0) = \mathcal{P}$, it is $\mathcal{N}_{ec, \mathcal{P}}(\Omega_0) = \mathcal{N}_{ec, \mathcal{P}}$. Since
 521 $z_{\xi_i \rightarrow B}(\cdot)$ acts as an identity operator on ξ_i , we have

$$\begin{aligned}
 522 \quad |I^h(\Psi \cdot (u - u_0))|_{a(B)}^2 &= \left| \sum_{\xi_i \in \mathcal{N}_{ec, \mathcal{P}}(\Omega_l)} z_{\xi_i \rightarrow B}(\Psi \cdot (u - u_0)) \right|_{a(B)}^2 \\
 523 &= \sum_{T \in \tau_h(B)} \left| \sum_{\xi_i \in \mathcal{N}_{ec, \mathcal{P}}(\Omega_l)} z_{\xi_i \rightarrow B}(\Psi \cdot (u - u_0)) \right|_{a(T)}^2. \\
 524
 \end{aligned}$$

525 There can be at most C_τ NECs ξ_i that are nonzero in any element T . Thus, we
 526 have using the Cauchy–Schwarz inequality

$$527 \quad \left| \sum_{\xi_i \in \mathcal{N}_{ec, \mathcal{P}}(\Omega_l)} z_{\xi_i \rightarrow B}(\Psi \cdot (u - u_0)) \right|_{a(T)}^2 \leq C_\tau \sum_{\xi_i \in \mathcal{N}_{ec, \mathcal{P}}(\Omega_l)} \left| z_{\xi_i \rightarrow B}(\Psi \cdot (u - u_0)) \right|_{a(T)}^2$$

529 and consequently

$$530 \quad |I^h(\Psi \cdot (u - u_0))|_{a(B)}^2 \leq C_\tau \sum_{\xi_i \in \mathcal{N}_{ec, \mathcal{P}}(\Omega_l)} \left| z_{\xi_i \rightarrow \Omega_{\xi_i}}(\Psi \cdot (u - u_0)) \right|_{a(\Omega_{\xi_i})}^2.$$

531

532 Since $0 \leq \Psi \leq 1$ is constant on a NEC $\xi_i \in \mathcal{N}_{ec, \mathcal{P}}(\Omega_l)$, we have

$$\begin{aligned}
533 \quad \sum_{\xi_i \in \mathcal{N}_{ec, \mathcal{P}}(\Omega_l)} \left| z_{\xi_i \rightarrow \Omega_{\xi_i}}(\Psi \cdot (u - u_0)) \right|_{a(\Omega_{\xi_i})}^2 &= \sum_{\xi_i \in \mathcal{N}_{ec, \mathcal{P}}(\Omega_l)} (\Psi|_{\xi_i})^2 \left| z_{\xi_i \rightarrow \Omega_{\xi_i}}(u - u_0) \right|_{a(\Omega_{\xi_i})}^2 \\
534 &\leq \sum_{\xi_i \in \mathcal{N}_{ec, \mathcal{P}}(\Omega_l)} \left| z_{\xi_i \rightarrow \Omega_{\xi_i}}(u - u_0) \right|_{a(\Omega_{\xi_i})}^2 \\
535 &\leq \sum_{\xi \in \mathcal{P}(\Omega_l)} \sum_{i=1}^{n_\xi} \left| z_{\xi_i \rightarrow \Omega_{\xi_i}}(u - u_0) \right|_{a(\Omega_{\xi_i})}^2 \\
536 &= \sum_{\xi \in \mathcal{P}(\Omega_l)} c_\xi(u - u_0, u - u_0). \\
537
\end{aligned}$$

538 Using [Lemma 11.1](#), we obtain

$$539 \quad C_\tau \sum_{\xi \in \mathcal{P}(\Omega_l)} c_\xi(u - u_0, u - u_0) \leq \frac{C_\tau}{\text{tol}_{\mathcal{P}}} \sum_{\xi \in \mathcal{P}(\Omega_l)} \sum_{k \in n^\xi} |u|_{a(\Omega_k)}^2.$$

540 Thus, in total, we have

$$541 \quad |I^h(\Psi \cdot (u - u_0))|_{a(B)}^2 \leq \frac{C_\tau}{\text{tol}_{\mathcal{P}}} \sum_{\xi \in \mathcal{P}(\Omega_l)} \sum_{k \in n^\xi} |u|_{a(\Omega_k)}^2.$$

542

□

543 Now, we are able to prove the existence of a stable decomposition.

544 **THEOREM 11.4 (Stable Decomposition).** *For each $u \in V^h(\Omega)$, there exists a*
545 *decomposition $u = \sum_{i=0}^N R_i^T u_i$, $u_i \in V_i = V^h(\Omega'_i)$, where $\Omega'_0 := \Omega$, such that*

$$546 \quad \sum_{i=0}^N |u_i|_{a(\Omega'_i)}^2 \leq C_0^2 |u|_{a(\Omega)}^2, \\
547$$

548 where $C_0^2 = \left(14 + (12N^\xi + C) \frac{C_\tau}{\text{tol}_{\mathcal{P}}}\right)$ and

$$549 \quad (11.3) \quad \mathcal{C} := \mathcal{C}(\{\Omega_i\}_{i=1}^N, \mathcal{P}) := \max_{1 \leq i \leq N} \sum_{j=1}^N |\{\xi \in \mathcal{P} : i, j \in n^\xi\}|.$$

550 \mathcal{C} is a measure for the \mathcal{P} -connectivity of the domain decomposition: Two subdomains
551 i, j are connected, if they touch the same interface component $\xi \in \mathcal{P}$, i.e., if $i, j \in n^\xi$.

552 *Proof.* On the overlapping decomposition $\{\tilde{\Omega}_i\}_{i=1}^N$ of width h , we consider the
553 local components $u_i := I^h(\theta_i \cdot (u - u_0))$ with the partition of unity $\{\theta_i\}_{i=1}^N$, $\theta_i : \{x^h \in \tilde{\Omega}\} \rightarrow \mathbb{R}$, where

$$554 \quad \theta_i(x^h) := \begin{cases} \frac{1}{|n(x^h)|} & \text{if } x^h \in \tilde{\Omega}_i, \\ 0 & \text{elsewhere,} \end{cases}$$

556 where x^h is a finite element node and $|n(x^h)|$ is the number of subdomains the node
557 x^h is contained in.

558 We note that, in general, $\{\tilde{\Omega}_i\}_{i=1}^N$ differs from the decomposition $\{\Omega'_i\}_{i=1}^N$ used
559 in the first level of the preconditioner, in which an overlap with one or more layers
560 of finite elements is used. The decomposition $\{\tilde{\Omega}_i\}_{i=1}^N$ is only used in the proof

561 and, since $\tilde{\Omega}_i \subset \Omega'_i$, we have $u_i \in V_i$. Thus, no restriction is placed on the size of
 562 the overlap of $\{\Omega'_i\}_{i=1}^N$. The condition number estimate in [Corollary 11.5](#) does not
 563 reflect the fact that the rate of convergence of the algorithm often improves when
 564 the overlap is increased.

565 We define the cutoff function $\theta : \{x^h \in \bar{\Omega}\} \rightarrow [0, 1]$ s.t.

$$566 \quad \theta(x^h) := 1 - \frac{1}{|n(x^h)|} \quad \text{for any node } x^h \in \bar{\Omega}.$$

567 Then, we have

$$\begin{aligned} 568 \quad |u_i|_{a(\Omega'_i)}^2 &= |u_i|_{a(\tilde{\Omega}_i)}^2 = |I^h(\theta_i(u - u_0))|_{a(\tilde{\Omega}_i)}^2 \\ 569 \quad &= |I^h(\theta_i(u - u_0))|_{a(\Omega_i)}^2 + |I^h(\theta_i(u - u_0))|_{a(\tilde{\Omega}_i \setminus \Omega_i)}^2 \\ 570 \quad &\leq 2|I^h((1 - \theta_i)(u - u_0))|_{a(\Omega_i)}^2 + 2|u - u_0|_{a(\Omega_i)}^2 + |I^h(\theta_i(u - u_0))|_{a(\tilde{\Omega}_i \setminus \Omega_i)}^2 \\ 571 \quad &\leq 2|I^h(\theta(u - u_0))|_{a(\Omega_i)}^2 + 4|u|_{a(\Omega_i)}^2 + 4|u_0|_{a(\Omega_i)}^2 + |I^h(\theta_i(u - u_0))|_{a(\tilde{\Omega}_i \setminus \Omega_i)}^2. \end{aligned}$$

573 As θ is only nonzero on Γ^h , it follows from [Lemma 11.3](#) that

$$\begin{aligned} 574 \quad \sum_{i=1}^N 2|I^h(\theta(u - u_0))|_{a(\Omega_i)}^2 &= 2|I^h(\theta(u - u_0))|_{a(\Omega)}^2 \\ 575 \quad &\leq 2\frac{C_\tau}{\text{tol}_{\mathcal{P}}} \sum_{\xi \in \mathcal{P}} \sum_{k \in n^\xi} |u|_{a(\Omega_k)}^2 \\ 576 \quad (11.4) \quad &\leq 2\frac{C_\tau N^\xi}{\text{tol}_{\mathcal{P}}} |u|_{a(\Omega)}^2. \end{aligned}$$

578 Similarly, we have

$$579 \quad (11.5) \quad \sum_{i=1}^N |I^h(\theta_i(u - u_0))|_{a(\tilde{\Omega}_i \setminus \Omega_i)}^2 \leq \frac{C_\tau}{\text{tol}_{\mathcal{P}}} \sum_{i=1}^N \sum_{\xi \in \mathcal{P}(\Omega_i)} \sum_{k \in n^\xi} |u|_{a(\Omega_k)}^2 \leq \mathcal{C} \frac{C_\tau}{\text{tol}_{\mathcal{P}}} |u|_{a(\Omega)}^2.$$

580 Thus, using [\(11.4\)](#), [\(11.5\)](#), and [Lemma 11.2](#), we obtain

$$\begin{aligned} 581 \quad \sum_{i=0}^N |u_i|_{a(\Omega'_i)}^2 &= |u_0|_{a(\Omega)}^2 + \sum_{i=1}^N |u_i|_{a(\tilde{\Omega}_i)}^2 \\ 582 \quad &\leq 5|u_0|_{a(\Omega)}^2 + 4|u|_{a(\Omega)}^2 + 2\frac{C_\tau N^\xi}{\text{tol}_{\mathcal{P}}} |u|_{a(\Omega)}^2 + \frac{C_\tau \mathcal{C}}{\text{tol}_{\mathcal{P}}} |u|_{a(\Omega)}^2 \\ 583 \quad &\leq 5 \cdot 2 \left(1 + \frac{C_\tau N^\xi}{\text{tol}_{\mathcal{P}}}\right) |u|_{a(\Omega)}^2 + \left(4 + (2N^\xi + \mathcal{C}) \frac{C_\tau}{\text{tol}_{\mathcal{P}}}\right) |u|_{a(\Omega)}^2 \\ 584 \quad &= \left(14 + (12N^\xi + \mathcal{C}) \frac{C_\tau}{\text{tol}_{\mathcal{P}}}\right) |u|_{a(\Omega)}^2. \quad \square \\ 585 \end{aligned}$$

586 From [Theorem 11.4](#), we directly obtain a condition number estimate for the pre-
 587 conditioned system.

588 **COROLLARY 11.5.** *The condition number of the RAGDSW two-level Schwarz*
 589 *operator in three dimensions is bounded by*

$$590 \quad \kappa(M_{\text{RAGDSW}}^{-1}K) \leq \left(14 + (12N^\xi + \mathcal{C}) \frac{C_\tau}{\text{tol}_{\mathcal{P}}}\right) (\hat{N}_c + 1),$$

592 where \hat{N}_c is an upper bound for the number of overlapping subdomains $\{\Omega'_i\}_{i=1}^N$ any
 593 point $x^h \in \Omega$ can belong to. All constants are independent of H , h , and the contrast
 594 of Young's modulus E .

595 *Proof.* Since we use exact local solvers, we directly obtain

$$596 \quad \kappa(M_{\text{RAGDSW}}^{-1}K) \leq C_0^2(\hat{N}_c + 1),$$

597 where C_0^2 is the constant of the stable decomposition; cf. [43, Lemma 3.11] and
 598 the follow-up discussion and the proof of [11, Theorem 4.1]. We obtain the final
 599 estimate using [Theorem 11.4](#). \square

600 **12. A variant using local Neumann problems.** We will now describe a
 601 technique that can significantly speed up the algorithm in a parallel setting and
 602 greatly facilitate its implementation.

603 We first consider the case of an interface component which is a coarse face f .
 604 The energy-minimal extension used in the generalized eigenvalue problem (9.7) is
 605 only weakly coupled between the two subdomains via the nodes adjacent to the
 606 face, i.e. $(\Gamma^h \cap \bar{\Omega}_i \cap \bar{\Omega}_j) \setminus f$ contains relatively few nodes on certain coarse edges
 607 and at certain coarse nodes. Instead of computing this coupled extension $\mathcal{H}_{f \rightarrow \Omega_f}(\cdot)$
 608 from the face f to the two adjacent subdomains as in (9.3), we can compute the
 609 extensions to each subdomain Ω_i, Ω_j separately. We expect that little information
 610 will be lost. We find that

$$611 \quad a_{\Omega_\xi}(\mathcal{H}_{\xi \rightarrow \Omega_\xi}(\theta), \mathcal{H}_{\xi \rightarrow \Omega_\xi}(\theta)) \geq \sum_{k \in n^\xi} a_{\Omega_k}(\mathcal{H}_{\xi \rightarrow \Omega_k}(\theta), \mathcal{H}_{\xi \rightarrow \Omega_k}(\theta)),$$

613 for $\theta \in X^h(\xi)$. Since the subdomains are only weakly coupled via these adjacent
 614 nodes of the face, we expect only a small change if we replace the left hand side
 615 of (9.7) using this alternative extension and that the dimension of the coarse space
 616 will increase only slightly.

617 The same technique can be applied to arbitrary interface components $\xi \in \mathcal{P}$.
 618 We might expect that the coupling will be stronger between subdomains for smaller
 619 interface components but our numerical results in [section 14](#) suggest that the in-
 620 crease in the coarse space dimension is moderate in all cases considered.

621 We indicate that this technique is employed by adding a trailing S to the coarse
 622 space name: $V_{\text{AGDSW-S}}$ and $V_{\text{RAGDSW-S}}$. Using this modification yields the same
 623 condition number bound as in [Corollary 11.5](#), since the modified $d_\xi(\cdot, \cdot), d_\xi^S(\cdot, \cdot)$,
 624 satisfies the same inequality as in (10.4):

$$625 \quad |v|_{d_\xi^S}^2 := d_\xi^S(v, v) := \sum_{k \in n^\xi} |\mathcal{H}_{\xi \rightarrow \Omega_k}(v)|_{a(\Omega_k)}^2 \leq \sum_{k \in n^\xi} |v|_{a(\Omega_k)}^2 = |v|_{a(\Omega_\xi)}^2 \quad \forall v \in V^h(\Omega).$$

626 Let the local (nonoverlapping) stiffness matrices with a Neumann boundary for
 627 the corresponding bilinear forms $a_{\Omega_i}(\cdot, \cdot)$ be given by K^{Ω_i} . For each $\xi \in \mathcal{P}$, we
 628 partition the degrees of freedom of Ω_i into those in $\xi \cap \bar{\Omega}_i$ and the remaining ones,
 629 R . We have

$$630 \quad K^{\Omega_i} = \begin{pmatrix} K_{RR}^{\Omega_i} & K_{R\xi}^{\Omega_i} \\ K_{\xi R}^{\Omega_i} & K_{\xi\xi}^{\Omega_i} \end{pmatrix}.$$

631 Let R_{ξ, Ω_k}^T map the degrees of freedom of $\xi \cap \bar{\Omega}_k$ to ξ . We define

$$632 \quad S_{\xi\xi}^S := \sum_{k \in n^\xi} R_{\xi, \Omega_k}^T S_{\xi\xi}^k,$$

633 with the Schur complements

$$634 \quad S_{\xi\xi}^k := K_{\xi\xi}^{\Omega_k} - K_{\xi R}^{\Omega_k} \left(K_{RR}^{\Omega_k} \right)^+ K_{R\xi}^{\Omega_k}, \quad k \in n^\xi,$$

635 where $(K_{RR}^{\Omega_k})^+$ is a pseudoinverse of $K_{RR}^{\Omega_k}$, cf. [Remark 9.1](#) and [section 13](#). Using the
 636 definition of $\tilde{K}_{\xi\xi}$ from [\(7.2\)](#), we obtain the modified generalized eigenvalue problem
 637 given in matrix form by

$$638 \quad S_{\xi\xi}^S \tau_{*,\xi} = \lambda_{*,\xi} \tilde{K}_{\xi\xi} \tau_{*,\xi}.$$

639 **13. Remarks on the computation of the energy-minimal extension.**

640 For an interface component $\xi \in \mathcal{P}$, the energy-minimal extension [\(9.3\)](#) satisfies
 641 a homogeneous Neumann boundary condition on $\partial\Omega_\xi \setminus \xi$. Therefore, for linear
 642 elasticity, if ξ consists only of a single node or if it is given by a straight edge,
 643 then all three rotations or the rotation around the edge are in the null space of
 644 the problem; cf. [Remark 9.1](#). Thus, in such cases, the operator $\mathcal{H}_{\xi \rightarrow \Omega_\xi}(\cdot)$ defined
 645 by [\(9.3\)](#) is symmetric and only positive semidefinite.

646 We also note that if the variant described in [section 12](#) is used, the extension
 647 operators are even more likely to be only positive semidefinite, since the extension
 648 is defined on the sets $\xi \cap \bar{\Omega}_k$, $k \in n^\xi$.

649 In an implementation, we have several options. Theoretically, we could compute
 650 a full pseudoinverse, however, this is very expensive in terms of processor time and
 651 memory. As an algebraic alternative, a pivoted factorization can be computed such
 652 that the diagonal is rank revealing. Alternatively, we can add a small regularization
 653 term $\varepsilon \mathcal{R}$ to obtain a symmetric, positive definite problem; e.g., $\varepsilon \mathcal{R} = 10^{-13} K_{\text{diag}}$,
 654 where K_{diag} is the diagonal of the respective matrix.

655 We have also considered two further, geometric approaches. One approach is to
 656 remove the null space by a projection. For this, we need to determine a basis of the
 657 null space, i.e., compute the rotations which requires geometric information. This
 658 approach has another downside, if we want to use a direct solver on the resulting
 659 system, since transforming the system is quite expensive and the transformed system
 660 is generally more dense.

661 A second geometric approach is less algebraic and eliminates a subset of the
 662 degrees of freedom of the matrix H corresponding to $\mathcal{H}_{\xi \rightarrow \Omega_\xi}(\cdot)$ at the expense of
 663 solving a small Schur complement system using a pseudoinverse. At best, this
 664 amounts to prescribing a zero Dirichlet boundary condition on some additional
 665 degrees of freedom. We partition the matrix H w.r.t. ξ and the remaining degrees
 666 of freedom R . To evaluate $\mathcal{H}_{\xi \rightarrow \Omega_\xi}(\cdot)$ requires the application of H_{RR}^{-1} . However,
 667 if ξ is a straight edge or a vertex, the submatrix H_{RR} has a null space of 1 or 3
 668 rotations.

669 In general, we pick as least as many degrees of freedom $\tilde{D} \subset R$ as the dimension
 670 of the null space of H_{RR} . Let the remaining degrees of freedom be denoted by
 671 $\tilde{R} \subset R$. The matrix H_{RR} is partitioned by \tilde{R} and \tilde{D} s.t.

$$672 \quad H_{RR} = \begin{pmatrix} H_{\tilde{R},\tilde{R}} & H_{\tilde{R},\tilde{D}} \\ H_{\tilde{D},\tilde{R}} & H_{\tilde{D},\tilde{D}} \end{pmatrix}.$$

673 The variables \tilde{R} are then eliminated to obtain a Schur complement system

$$674 \quad \begin{pmatrix} H_{\tilde{R},\tilde{R}} & H_{\tilde{R},\tilde{D}} \\ 0 & S_{\tilde{D},\tilde{D}} \end{pmatrix}, \quad S_{\tilde{D},\tilde{D}} = H_{\tilde{D},\tilde{D}} - H_{\tilde{D},\tilde{R}} H_{\tilde{R},\tilde{R}}^{-1} H_{\tilde{R},\tilde{D}}.$$

675 If \tilde{D} was chosen properly, the submatrix $H_{\tilde{R},\tilde{R}}$ is invertible. For example, if ξ is a
 676 straight edge and \tilde{D} corresponds to a node which does not lie on the same straight
 677 as the edge (note that three degrees of freedom are associated with each node), then
 678 $H_{\tilde{R},\tilde{R}}$ is invertible. In that case, the Schur complement is well defined and has a
 679 null space of the same dimension as H_{RR} . Thus, we can solve the corresponding

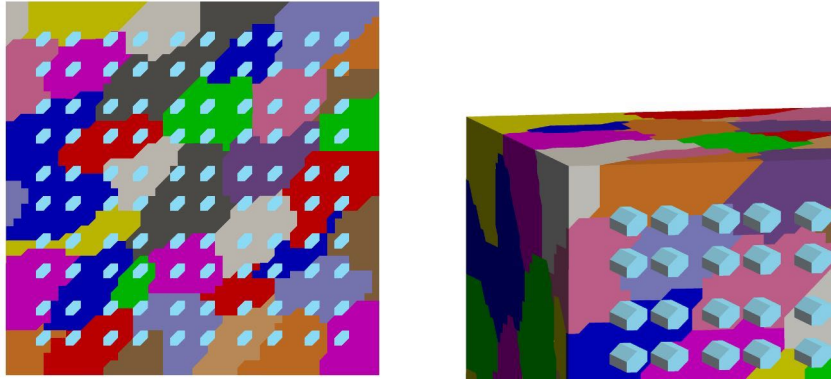


FIG. 5. Cross section (left) of a domain decomposition of a cube and a discontinuous coefficient function E with beams of large coefficients (light blue) crossing the domain. The beams of large coefficients do not touch the domain boundary. The light blue color corresponds to a coefficient of $E_{\max} = 10^6$ and the remainder is set to $E_{\min} = 1.0$. Number of subdomains: 125; number of nodes: 132651 (degrees of freedom: 397953); average degrees of freedom per overlapping subdomain: 6198; overlap: two layers of finite elements. Structured tetrahedral mesh; unstructured domain decomposition (METIS). For the corresponding results, see Table 2. Taken from [21, Figure 8].

680 system using a pseudoinverse. This is much cheaper than using a pseudoinverse on
 681 K_{RR} , since $S_{\tilde{D},\tilde{D}}$ is of a much smaller dimension than K_{RR} .

682 If we select the degrees of freedom in \tilde{D} carefully, the Schur complement will
 683 be identically zero, i.e., evaluating $\mathcal{H}_{\xi \rightarrow \Omega_\xi}(\cdot)$ is no more expensive than solving a
 684 linear system with $K_{\tilde{R},\tilde{R}}$ and the cost will be comparable to that of a case with an
 685 invertible K_{RR} .

686 **14. Numerical results.** In this section, we present numerical results to com-
 687 pare the nonadaptive coarse spaces GDSW and RGDSW, the adaptive coarse spaces
 688 AGDSW (section 5) and RAGDSW (section 8), and their S-variants AGDSW-S and
 689 RAGDSW-S; cf. section 12.

690 We show numerical results for a discretization of problem (2.1) with a Pois-
 691 son ratio $\nu = 0.4$, the right hand side $f \equiv (1, 1, 1)^T$, and several coefficient func-
 692 tions given by different choices of the Young modulus function $E(\cdot)$. The small-
 693 est Young modulus $E_{\min} := \min_{x \in \Omega} E(x)$ is always set to 1 and the maximum
 694 $E_{\max} := \max_{x \in \Omega} E(x)$ is specified in the respective figure and table caption. Ex-
 695 cept for the test case of Figure 6 and Table 3, the computational domain is the unit
 696 cube with a zero Dirichlet condition prescribed on all its boundary.

697 We use piecewise linear basis functions on tetrahedra and we solve the resulting
 698 linear system with the preconditioned conjugate gradient (PCG) method and a
 699 relative stopping criterion of $\|r^{(k)}\|_2 / \|r^{(0)}\|_2 < 10^{-8}$, where $r^{(0)}$ and $r^{(k)}$ are the
 700 initial and the k th unpreconditioned residuals. The reported condition numbers
 701 are the estimates obtained after the last iteration of the PCG method using the
 702 Lanczos method [39, Chapter 6.7.3]. We partition the domain into subdomains
 703 using METIS [29]. In all experiments, we use an overlap of two layers of finite
 704 elements; see section 3 for the definition of the overlap.

705 The coefficient function of the first test problem is depicted in Figure 5; the
 706 corresponding results are given in Table 2. Experiments with both nonadaptive
 707 coarse spaces GDSW and RGDSW failed to converge in 2000 iterations, clearly
 708 showing that adaptivity is required to obtain a robust preconditioner. By using
 709 the adaptive coarse spaces, we obtain acceptable condition numbers and iteration
 710 counts. The results show a significant reduction in the coarse space dimension for the
 711 RAGDSW variant compared to AGDSW. For example ($tol = 0.05$), the dimension

TABLE 2

Results for the coefficient function in Figure 5: iteration counts, condition numbers, and resulting coarse space dimension for different coarse spaces. Number of subdomains: 125; degrees of freedom: 397953; overlap: two layers of finite elements; maximum coefficient $E_{\max} = 10^6$; relative stopping criterion $\|r^{(k)}\|_2/\|r^{(0)}\|_2 < 10^{-8}$. Structured tetrahedral mesh; unstructured domain decomposition (METIS).

V_0	Coefficient function E from Figure 5					
	tol	it.	κ	$\dim V_0$	$(\mathcal{V}/\mathcal{P}, \mathcal{E}, \mathcal{F})$	$\dim V_0/\text{dof}$
V_{GDSW}	–	>2000	$3.1 \cdot 10^5$	9996	(1707, 4618, 3671)	2.51%
V_{RGDSW}	–	>2000	$3.9 \cdot 10^5$	3358	(3358, 0, 0)	0.84%
V_{AGDSW}	0.100	71	41.1	14439	(1707, 4943, 7789)	3.63%
V_{AGDSW}	0.050	90	59.5	13945	(1707, 4915, 7323)	3.50%
V_{AGDSW}	0.010	132	161.1	13763	(1707, 4912, 7144)	3.46%
V_{AGDSW}	0.001	327	971.8	13721	(1707, 4907, 7107)	3.45%
$V_{\text{AGDSW-S}}$	0.100	63	28.7	14597	(1707, 5020, 7870)	3.67%
$V_{\text{AGDSW-S}}$	0.050	89	57.5	14004	(1707, 4949, 7348)	3.52%
$V_{\text{AGDSW-S}}$	0.010	134	166.0	13767	(1707, 4914, 7146)	3.46%
$V_{\text{AGDSW-S}}$	0.001	305	973.1	13729	(1707, 4911, 7111)	3.45%
V_{RAGDSW}	0.100	67	34.6	8249	(8249, 0, 0)	2.07%
V_{RAGDSW}	0.050	88	61.3	7683	(7683, 0, 0)	1.93%
V_{RAGDSW}	0.010	114	117.4	7501	(7501, 0, 0)	1.88%
V_{RAGDSW}	0.001	383	$1.4 \cdot 10^3$	7401	(7401, 0, 0)	1.86%
$V_{\text{RAGDSW-S}}$	0.100	62	32.7	8799	(8799, 0, 0)	2.21%
$V_{\text{RAGDSW-S}}$	0.050	79	51.4	7903	(7903, 0, 0)	1.99%
$V_{\text{RAGDSW-S}}$	0.010	109	104.5	7563	(7563, 0, 0)	1.90%
$V_{\text{RAGDSW-S}}$	0.001	268	902.7	7525	(7525, 0, 0)	1.89%

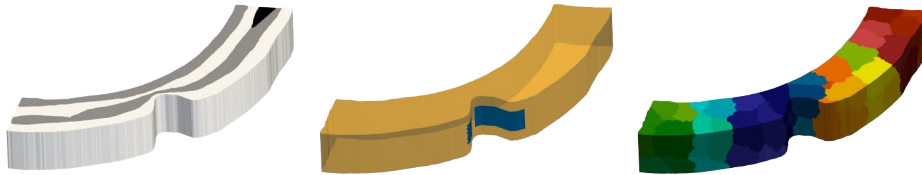


FIG. 6. (left) Discontinuous coefficient function E with coefficient layers of $E = 10^6$ in light gray and an inclusion at the top right with $E = 10^9$ in dark gray. The remainder of the coefficient in white is set to $E_{\min} = 1.0$. (center) Boundary partition for Dirichlet (blue) and Neumann (orange) boundary. (right) Domain decomposition of 50 subdomains. Number of nodes: 56053 (degrees of freedom: 168159); average degrees of freedom per overlapping subdomain: 5632.2; overlap: two layers of finite elements. Unstructured tetrahedral mesh; unstructured domain decomposition (METIS). For the corresponding results, see Table 3. Taken from [21, Figure 9].

712 of $V_{\text{AGDSW-S}}$ is reduced by 43.6% by using $V_{\text{RAGDSW-S}}$. And even while GDSW
 713 does not converge in 2000 iterations, its coarse space is 26.5% larger than that of
 714 RAGDSW-S ($tol = 0.05$).

715 For the next example, we consider a problem, for which we impose a Neu-
 716 mann boundary condition on most of the domain boundary; see Figure 6. The
 717 results in Table 3 show an even larger reduction in the coarse space dimension from
 718 AGDSW to RAGDSW compared to the previous case. We obtain a reduction of
 719 69.4% ($tol = 0.05$). The reason for this is the larger number of interface com-
 720 ponents: Since the AGDSW space contains the GDSW space and the RAGDSW
 721 space contains the RGDSW space, a significant part of the coarse space reduc-
 722 tion can be attributed to the smaller dimension of RGDSW compared to GDSW.
 723 This highlights the core idea behind the reduced dimension GDSW spaces in [9];
 724 the explanation is supported by the fact that the dimension of V_{RAGDSW} is fairly
 725 close to that of V_{RGDSW} . Therefore, since the coefficient function contains only
 726 relatively few connected large coefficient components, only a few additional coarse
 727 basis functions are required.

TABLE 3

Results for the coefficient function in Figure 6: iteration counts, condition numbers, and resulting coarse space dimension for different coarse spaces. Number of subdomains: 50; degrees of freedom: 168 159; overlap: two layers of finite elements; maximum coefficient $E_{\max} = 10^9$; relative stopping criterion $\|r^{(k)}\|_2/\|r^{(0)}\|_2 < 10^{-8}$. Unstructured tetrahedral mesh; unstructured domain decomposition (METIS).

V_0	Coefficient function E from Figure 6					
	tol	it.	κ	$\dim V_0$	$(\mathcal{V}/\mathcal{P}, \mathcal{E}, \mathcal{F})$	$\dim V_0/\text{dof}$
V_{GDSW}	–	1 329	$1.5 \cdot 10^7$	2 319	(291, 1 000, 1 028)	1.38%
V_{RGDSW}	–	1 549	$1.0 \cdot 10^7$	572	(572, 0, 0)	0.34%
V_{AGDSW}	0.100	60	20.2	2 732	(291, 1 058, 1 383)	1.62%
V_{AGDSW}	0.050	69	28.1	2 631	(291, 1 058, 1 282)	1.56%
V_{AGDSW}	0.010	71	28.2	2 626	(291, 1 058, 1 277)	1.56%
V_{AGDSW}	0.001	152	1 162.2	2 613	(291, 1 052, 1 270)	1.55%
$V_{\text{AGDSW-S}}$	0.100	58	18.9	2 741	(291, 1 059, 1 391)	1.63%
$V_{\text{AGDSW-S}}$	0.050	69	28.1	2 631	(291, 1 058, 1 282)	1.56%
$V_{\text{AGDSW-S}}$	0.010	72	28.2	2 626	(291, 1 058, 1 277)	1.56%
$V_{\text{AGDSW-S}}$	0.001	142	733.7	2 614	(291, 1 053, 1 270)	1.55%
V_{RAGDSW}	0.100	68	27.1	988	(988, 0, 0)	0.59%
V_{RAGDSW}	0.050	85	43.8	804	(804, 0, 0)	0.48%
V_{RAGDSW}	0.010	100	88.5	781	(781, 0, 0)	0.46%
V_{RAGDSW}	0.001	183	769.1	774	(774, 0, 0)	0.46%
$V_{\text{RAGDSW-S}}$	0.100	60	20.7	1 152	(1 152, 0, 0)	0.69%
$V_{\text{RAGDSW-S}}$	0.050	78	35.2	868	(868, 0, 0)	0.52%
$V_{\text{RAGDSW-S}}$	0.010	100	87.6	790	(790, 0, 0)	0.47%
$V_{\text{RAGDSW-S}}$	0.001	115	141.1	786	(786, 0, 0)	0.47%

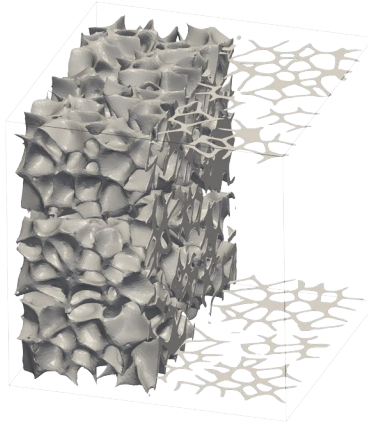


FIG. 7. Partial visualization of an unstructured tetrahedral mesh consisting of several disconnected components of foam-like structures. On the corresponding mesh of a cube, foam corresponds to a large coefficient of $E_{\max} = 10^6$ with $E_{\min} = 1.0$ elsewhere. The large coefficient does not touch the domain boundary. Number of subdomains: 100; number of nodes: 588 958 (degrees of freedom: 1 766 874); average degrees of freedom per overlapping subdomain: 19 969.2; overlap: two layers of finite elements. Unstructured tetrahedral mesh; unstructured domain decomposition (METIS). For the corresponding results, see Table 4. Taken from [21, Figure 10].

728 We consider another realistic geometry in Figure 7 with a foamlike structure.
 729 We note that the foam is not a single connected structure but consists of several
 730 smaller disconnected foamlike structures. The results in Table 4 are similar to the
 731 previous ones. By using RAGDSW-S, we obtain a coarse space reduction of 49.9%
 732 compared to AGDSW-S ($tol = 0.05$). However, here, the dimension of $V_{\text{RAGDSW-S}}$
 733 is more than double that of V_{RGDSW} indicating that $V_{\text{RAGDSW-S}}$ is adaptively
 734 enriched with quite a few additional basis functions compared to V_{RGDSW} .

735 We conclude with averaged results for 100 random coefficient functions showing

TABLE 4

Results for the coefficient function in Figure 7: iteration counts, condition numbers, and resulting coarse space dimension for different coarse spaces. Number of subdomains: 100; degrees of freedom: 1766874; overlap: two layers of finite elements; maximum coefficient $E_{\max} = 10^6$; relative stopping criterion $\|r^{(k)}\|_2/\|r^{(0)}\|_2 < 10^{-8}$. Unstructured tetrahedral mesh; unstructured domain decomposition (METIS).

V_0	Coefficient function E from Figure 7					
	tol	it.	κ	$\dim V_0$	$(\mathcal{V}/\mathcal{P}, \mathcal{E}, \mathcal{F})$	$\dim V_0/\text{dof}$
V_{GDSW}	–	1865	$1.1 \cdot 10^6$	8311	(1167, 4108, 3036)	0.47%
V_{RGDSW}	–	1613	$9.3 \cdot 10^5$	2313	(2313, 0, 0)	0.13%
V_{AGDSW}	0.10	52	21.4	12367	(1167, 4358, 6842)	0.70%
V_{AGDSW}	0.05	68	43.8	10940	(1167, 4351, 5422)	0.62%
V_{AGDSW}	0.01	167	333.4	10304	(1167, 4324, 4813)	0.58%
$V_{\text{AGDSW-S}}$	0.10	50	18.7	12539	(1167, 4389, 6983)	0.71%
$V_{\text{AGDSW-S}}$	0.05	63	32.2	11005	(1167, 4362, 5476)	0.62%
$V_{\text{AGDSW-S}}$	0.01	147	158.1	10320	(1167, 4338, 4815)	0.58%
V_{RAGDSW}	0.10	54	22.0	6641	(6641, 0, 0)	0.38%
V_{RAGDSW}	0.05	80	45.2	4868	(4868, 0, 0)	0.28%
V_{RAGDSW}	0.01	189	280.2	4019	(4019, 0, 0)	0.23%
$V_{\text{RAGDSW-S}}$	0.10	50	18.4	7833	(7833, 0, 0)	0.44%
$V_{\text{RAGDSW-S}}$	0.05	69	46.1	5519	(5519, 0, 0)	0.31%
$V_{\text{RAGDSW-S}}$	0.01	151	202.6	4152	(4152, 0, 0)	0.23%

TABLE 5

Averaged results for 100 random coefficient functions (average large coefficient density: 11.08%): tolerance for the selection of the eigenfunctions, iteration counts, condition numbers, and resulting coarse space dimension for different coarse spaces; maximum in brackets. Number of subdomains: 512; number of nodes: 452522 (degrees of freedom: 1357566); average degrees of freedom per overlapping subdomain: 5906.4; overlap: two layers of finite elements; maximum coefficient $E_{\max} = 10^6$; relative stopping criterion $\|r^{(k)}\|_2/\|r^{(0)}\|_2 < 10^{-8}$. Unstructured tetrahedral mesh; unstructured domain decomposition (METIS). V_{GDSW} and V_{RGDSW} never converged in 2000 iterations.

V_0	Random coefficient function E					
	tol	it.	κ	$\dim V_0$	$\dim V_0/\text{dof}$	
V_{GDSW}	–	>2000 (–)	$2.1 \cdot 10^5$ ($3.2 \cdot 10^5$)	49862.0 (49862)	3.7% (3.7%)	
V_{RGDSW}	–	>2000 (–)	$2.4 \cdot 10^5$ ($3.7 \cdot 10^5$)	17778.0 (17778)	1.3% (1.3%)	
V_{AGDSW}	0.10	84.8 (93)	56.2 (80.7)	69006.7 (69892)	5.1% (5.1%)	
	0.05	106.3 (118)	92.1 (145.2)	66482.5 (67273)	4.9% (5.0%)	
	0.01	180.8 (228)	293.3 (662.9)	64508.1 (65235)	4.8% (4.8%)	
$V_{\text{AGDSW-S}}$	0.10	76.4 (84)	44.1 (54.2)	70570.8 (71632)	5.2% (5.3%)	
	0.05	99.3 (112)	77.9 (110.7)	67445.3 (68360)	5.0% (5.0%)	
	0.01	168.1 (195)	247.5 (448.4)	65212.8 (66046)	4.8% (4.9%)	
V_{RAGDSW}	0.10	89.5 (100)	60.9 (82.2)	39081.8 (39780)	2.9% (2.9%)	
	0.05	115.1 (129)	104.8 (152.5)	35961.4 (36649)	2.6% (2.7%)	
	0.01	200.3 (232)	342.8 (523.6)	33370.8 (34058)	2.5% (2.5%)	
$V_{\text{RAGDSW-S}}$	0.10	74.9 (88)	42.8 (59.6)	44045.9 (44677)	3.2% (3.3%)	
	0.05	97.1 (112)	72.9 (103.5)	39076.9 (39730)	2.9% (2.9%)	
	0.01	167.8 (199)	244.7 (469.9)	35399.8 (36137)	2.6% (2.7%)	

736 the robustness of the methods; cf. Table 5. Despite comparable number of iterations
737 and condition numbers, the coarse space dimensions of RAGDSW(–S) are smaller
738 by a factor of 1.6 compared to those of AGDSW(–S) (at an equal tolerance).

739 **Acknowledgments.** We thank the Regional Computing Center of the Univer-
740 sity of Cologne (RRZK) for providing computing time on the DFG-funded High Per-
741 formance Computing (HPC) system CHEOPS (DFG FKZ: INST 216/512/1FUGG)
742 as well as support.

- 744 [1] J. AARNES AND T. Y. HOU, *Multiscale domain decomposition methods for elliptic problems*
745 *with high aspect ratios*, Acta Math. Appl. Sin. Engl. Ser., 18 (2002), pp. 63–76.
- 746 [2] P. BJØRSTAD, J. KOSTER, AND P. KRZYZANOWSKI, *Domain decomposition solvers for large*
747 *scale industrial finite element problems*, in Applied Parallel Computing, New Paradigms
748 for HPC in Industry and Academia, vol. 1947 of Lect. Notes Comput. Sci., Springer,
749 Berlin, Heidelberg, 2001, pp. 373–383.
- 750 [3] M. BUCK, O. ILIEV, AND H. ANDRĂ, *Multiscale finite elements for linear elasticity: Oscilla-*
751 *tory boundary conditions*, in Domain Decomposition Methods in Science and Engineering
752 XXI, vol. 98 of Lect. Notes Comput. Sci. Eng., Springer, Cham, 2014, pp. 237–245.
- 753 [4] C. DOHRMANN AND O. B. WIDLUND, *An alternative coarse space for irregular subdomains*
754 *and an overlapping Schwarz algorithm for scalar elliptic problems in the plane*, SIAM
755 J. Numer. Anal., 50 (2012), pp. 2522–2537.
- 756 [5] C. R. DOHRMANN, A. KLAWONN, AND O. B. WIDLUND, *Domain decomposition for less regular*
757 *subdomains: Overlapping Schwarz in two dimensions*, SIAM J. Numer. Anal., 46 (2008),
758 pp. 2153–2168.
- 759 [6] C. R. DOHRMANN, A. KLAWONN, AND O. B. WIDLUND, *A family of energy minimizing coarse*
760 *spaces for overlapping Schwarz preconditioners*, in Domain Decomposition Methods in
761 Science and Engineering XVII, vol. 60 of Lect. Notes Comput. Sci. Eng., Springer, Berlin,
762 2008, pp. 247–254.
- 763 [7] C. R. DOHRMANN AND O. B. WIDLUND, *An overlapping Schwarz algorithm for almost in-*
764 *compressible elasticity*, SIAM J. Numer. Anal., 47 (2009), pp. 2897–2923.
- 765 [8] C. R. DOHRMANN AND O. B. WIDLUND, *Hybrid domain decomposition algorithms for com-*
766 *pressible and almost incompressible elasticity*, Internat. J. Numer. Meth. Engng., 82
767 (2010), pp. 157–183.
- 768 [9] C. R. DOHRMANN AND O. B. WIDLUND, *On the design of small coarse spaces for domain*
769 *decomposition algorithms*, SIAM J. Sci. Comput., 39 (2017), pp. A1466–A1488.
- 770 [10] V. DOLEAN, F. NATAF, R. SCHEICHL, AND N. SPILLANE, *Analysis of a two-level Schwarz*
771 *method with coarse spaces based on local Dirichlet-to-Neumann maps*, Comput. Methods
772 Appl. Math., 12 (2012), pp. 391–414.
- 773 [11] M. DRYJA AND O. B. WIDLUND, *Domain decomposition algorithms with small overlap*, SIAM
774 J. Sci. Comput., 15 (1994), pp. 604–620.
- 775 [12] Y. EFENDIEV AND T. Y. HOU, *Multiscale Finite Element Methods: Theory and Applications*,
776 Surv. Tutor. Appl. Math. Sci., Springer, New York, 2009.
- 777 [13] E. EIKELAND, L. MARCINKOWSKI, AND T. RAHMAN, *Overlapping Schwarz methods with*
778 *adaptive coarse spaces for multiscale problems in 3D*, Numer. Math, (2018).
- 779 [14] J. GALVIS AND Y. EFENDIEV, *Domain decomposition preconditioners for multiscale flows*
780 *in high contrast media: Reduced dimension coarse spaces*, Multiscale Model. Simul., 8
781 (2010), pp. 1621–1644.
- 782 [15] M. J. GANDER, A. LONELAND, AND T. RAHMAN, *Analysis of a new harmonically enriched*
783 *multiscale coarse space for domain decomposition methods*, 2015, [https://arxiv.org/abs/](https://arxiv.org/abs/1512.05285)
784 [1512.05285](https://arxiv.org/abs/1512.05285).
- 785 [16] A. HEINLEIN, *Parallel Overlapping Schwarz Preconditioners and Multiscale Discretizations*
786 *with Applications to Fluid-Structure Interaction and Highly Heterogeneous Problems*,
787 PhD thesis, University of Cologne, Cologne, Germany, 2016.
- 788 [17] A. HEINLEIN, C. HOCHMUTH, AND A. KLAWONN, *Monolithic overlapping Schwarz domain*
789 *decomposition methods with GDSW coarse spaces for incompressible fluid flow problems*,
790 SIAM J. Sci. Comp., 41 (2019), pp. C291–C316.
- 791 [18] A. HEINLEIN, C. HOCHMUTH, AND A. KLAWONN, *Reduced dimension GDSW coarse spaces*
792 *for monolithic Schwarz domain decomposition methods for incompressible fluid flow*
793 *problems*, Int. J. Numer. Meth. Eng., 121 (2020), pp. 1101–1119.
- 794 [19] A. HEINLEIN, A. KLAWONN, J. KNEPPER, AND O. RHEINBACH, *An adaptive GDSW coarse*
795 *space for two-level overlapping Schwarz methods in two dimensions*, in Domain Decom-
796 position Methods in Science and Engineering XXIV, vol. 125 of Lect. Notes Comput.
797 Sci. Eng., Springer, Cham, 2018, pp. 373–382.
- 798 [20] A. HEINLEIN, A. KLAWONN, J. KNEPPER, AND O. RHEINBACH, *Multiscale coarse spaces for*
799 *overlapping Schwarz methods based on the ACMS space in 2D*, Electron. Trans. Numer.
800 Anal., 48 (2018), pp. 156–182.
- 801 [21] A. HEINLEIN, A. KLAWONN, J. KNEPPER, AND O. RHEINBACH, *Adaptive GDSW coarse spaces*
802 *for overlapping Schwarz methods in three dimensions*, SIAM J. Sci. Comp., 41 (2019),
803 pp. A3045–A3072.
- 804 [22] A. HEINLEIN, A. KLAWONN, S. RAJAMANICKAM, AND O. RHEINBACH, *FROSch: A fast and*
805 *robust overlapping Schwarz domain decomposition preconditioner based on Xpetra in*
806 *Trilinos*, in Domain Decomposition Methods in Science and Engineering XXV, Lect.
807 Notes Comput. Sci. Eng., Springer, Cham, 2019. Accepted April 2019 for publication,
808 preprint CDS-TR 2018-9 <https://kups.uni-koeln.de/id/eprint/9018>.
- 809 [23] A. HEINLEIN, A. KLAWONN, AND O. RHEINBACH, *A parallel implementation of a two-level*
810 *overlapping Schwarz method with energy-minimizing coarse space based on Trilinos*,

- 811 SIAM J. Sci. Comput., 38 (2016), pp. C713–C747.
- 812 [24] A. HEINLEIN, A. KLAWONN, AND O. RHEINBACH, *Parallel two-level overlapping Schwarz*
813 *methods in fluid-structure interaction*, in Numerical Mathematics and Advanced Appli-
814 *cations ENUMATH 2015*, vol. 112 of Lect. Notes Comput. Sci. Eng., Springer, Cham,
815 2016, pp. 521–530.
- 816 [25] A. HEINLEIN, A. KLAWONN, AND O. RHEINBACH, *Parallel overlapping Schwarz with an*
817 *energy-minimizing coarse space*, in Domain Decomposition Methods in Science and En-
818 *gineering XXIII*, vol. 116 of Lect. Notes Comput. Sci. Eng., Springer, Cham, 2017,
819 pp. 353–360.
- 820 [26] A. HEINLEIN, A. KLAWONN, O. RHEINBACH, AND F. RÖVER, *A three-level extension of the*
821 *GDSW overlapping Schwarz preconditioner in three dimensions*, in Domain Decom-
822 *position Methods in Science and Engineering XXV*, Lect. Notes Comput. Sci. Eng.,
823 Springer, Cham, 2019. Accepted March 2019 for publication, preprint CDS-TR 2018-8
824 <https://kups.uni-koeln.de/id/eprint/9017>.
- 825 [27] A. HEINLEIN, A. KLAWONN, O. RHEINBACH, AND O. WIDLUND, *Improving the parallel per-*
826 *formance of overlapping Schwarz methods by using a smaller energy minimizing coarse*
827 *space*, in Domain Decomposition Methods in Science and Engineering XXIV, vol. 125 of
828 Lect. Notes Comput. Sci. Eng., Springer, Cham, 2019, pp. 383–392.
- 829 [28] T. Y. HOU AND X.-H. WU, *A multiscale finite element method for elliptic problems in*
830 *composite materials and porous media*, J. Comput. Phys., 134 (1997), pp. 169 – 189.
- 831 [29] G. KARYPIS AND V. KUMAR, *A fast and high quality multilevel scheme for partitioning*
832 *irregular graphs*, SIAM J. Sci. Comput., 20 (1998), pp. 359–392.
- 833 [30] H. H. KIM, E. CHUNG, AND J. WANG, *BDDC and FETI-DP preconditioners with adaptive*
834 *coarse spaces for three-dimensional elliptic problems with oscillatory and high contrast*
835 *coefficients*, J. Comput. Phys., 349 (2017), pp. 191–214.
- 836 [31] A. KLAWONN, M. KÜHN, AND O. RHEINBACH, *Adaptive coarse spaces for FETI-DP in three*
837 *dimensions*, SIAM J. Sci. Comput., 38 (2016), pp. A2880–A2911.
- 838 [32] A. KLAWONN, M. KÜHN, AND O. RHEINBACH, *Adaptive FETI-DP and BDDC methods with a*
839 *generalized transformation of basis for heterogeneous problems*, Electron. Trans. Numer.
840 Anal., 49 (2018), pp. 1–27.
- 841 [33] A. KLAWONN, P. RADTKE, AND O. RHEINBACH, *A comparison of adaptive coarse spaces for*
842 *iterative substructuring in two dimensions*, Electron. Trans. Numer. Anal., 45 (2016),
843 pp. 75–106.
- 844 [34] J. MANDEL AND B. SOUSEDÍK, *Adaptive selection of face coarse degrees of freedom in the*
845 *BDDC and the FETI-DP iterative substructuring methods*, Comput. Methods Appl.
846 Mech. Engrg., 196 (2007), pp. 1389–1399.
- 847 [35] J. MANDEL, B. SOUSEDÍK, AND J. ŠÍSTEK, *Adaptive BDDC in three dimensions*, Math.
848 Comput. Simulation, 82 (2012), pp. 1812–1831.
- 849 [36] L. MARCINKOWSKI AND T. RAHMAN, *Additive average Schwarz with adaptive coarse spaces:*
850 *Scalable algorithms for multiscale problems*, Electron. Trans. Numer. Anal., 49 (2018),
851 pp. 28–40.
- 852 [37] C. PECHSTEIN AND C. DOHRMANN, *Modern domain decomposition solvers—BDDC, deluxe*
853 *scaling, and an algebraic approach*. Slides to a talk at NuMa Seminar, JKU Linz, De-
854 cember 10, 2013, <http://people.ricam.oeaw.ac.at/c.pechstein/pechstein-bddc2013.pdf>.
- 855 [38] C. PECHSTEIN AND C. R. DOHRMANN, *A unified framework for adaptive BDDC*, Electron.
856 Trans. Numer. Anal., 46 (2017), pp. 273–336.
- 857 [39] Y. SAAD, *Iterative Methods for Sparse Linear Systems*, SIAM, second ed., 2003.
- 858 [40] B. SMITH, P. BJØRSTAD, AND W. GROPP, *Domain Decomposition: Parallel Multilevel Meth-*
859 *ods for Elliptic Partial Differential Equations*, Cambridge University Press, Cambridge,
860 1996.
- 861 [41] N. SPILLANE, V. DOLEAN, P. HAURET, F. NATAF, C. PECHSTEIN, AND R. SCHEICHL, *Abstract*
862 *robust coarse spaces for systems of PDEs via generalized eigenproblems in the overlaps*,
863 Numer. Math., 126 (2014), pp. 741–770.
- 864 [42] N. SPILLANE AND D. RIXEN, *Automatic spectral coarse spaces for robust finite element tear-*
865 *ing and interconnecting and balanced domain decomposition algorithms*, Int. J. Numer.
866 Meth. Eng., 95 (2013), pp. 953–990.
- 867 [43] A. TOSELLI AND O. WIDLUND, *Domain Decomposition Methods—Algorithms and Theory*,
868 vol. 34 of Springer Ser. Comput. Math, Springer, Berlin, Heidelberg, 2005.